Article

Cell

Competing Protein-RNA Interaction Networks Control Multiphase Intracellular Organization

Graphical Abstract

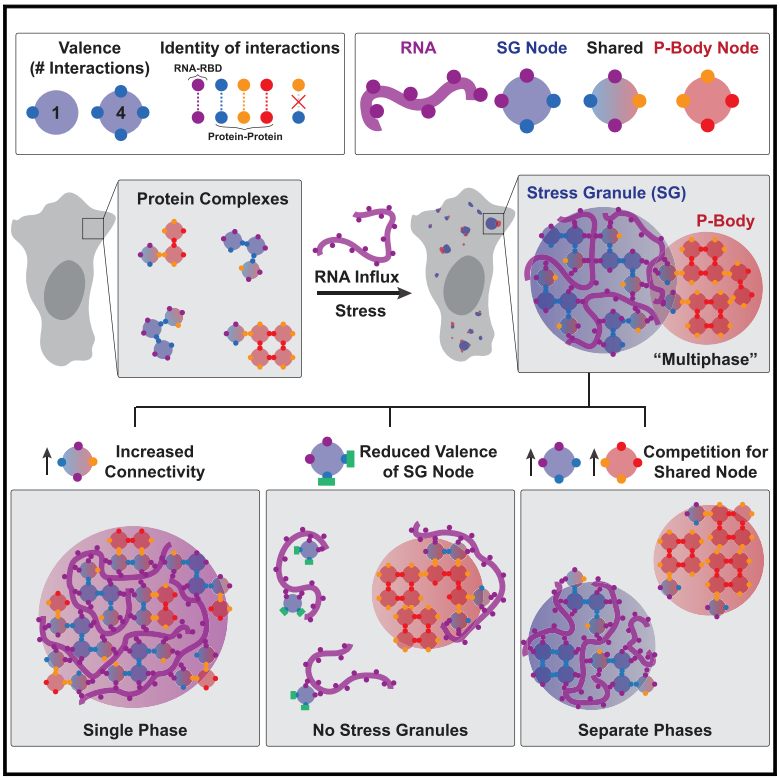

Highlights

- Stress granule formation requires RNA-binding nodes with high network connectivity
- Capping of nodes by ligands lacking connectivity prevents condensation
- Protein disorder and RNA-binding specificity play non-essential, modulatory roles
- Competition of RNP networks for connecting nodes controls multiphase organization

Authors

David W. Sanders, Nancy Kedersha, Daniel S.W. Lee, ..., William M. Jacobs, Pavel Ivanov, Clifford P. Brangwynne

Correspondence

cbrangwy@princeton.edu

In Brief

With sufficient RNA-binding interfaces, diverse protein complexes can trigger stress-dependent multiphase condensates, whose composition and spatial organization is determined by overlapping interaction networks.

Sanders et al., 2020, Cell *181*, 306–324
April 16, 2020
https://doi.org/10.1016/j.cell.2020.03.050

CellPress

Cell

Article

Competing Protein-RNA Interaction Networks Control Multiphase Intracellular Organization

David W. Sanders,[1] Nancy Kedersha,[4,6] Daniel S.W. Lee,[1,6] Amy R. Strom,[1,6] Victoria Drake,[1] Joshua A. Riback,[1] Dan Bracha,[1] Jorine M. Eeftens,[1] Allana Iwanicki,[1] Alicia Wang,[1] Ming-Tzo Wei,[1] Gena Whitney,[1] Shawn M. Lyons,[5] Paul Anderson,[4] William M. Jacobs,[2] Pavel Ivanov,[4] and Clifford P. Brangwynne[1,3,7,*]

[1]Department of Chemical and Biological Engineering, Princeton University, Princeton, NJ 08544, USA
[2]Department of Chemistry, Princeton University, Princeton, NJ 08544, USA
[3]Howard Hughes Medical Institute, Princeton, NJ 08544, USA
[4]Division of Rheumatology, Inflammation, and Immunity, Brigham and Women's Hospital and Harvard Medical School, Boston, MA 02115, USA
[5]Department of Biochemistry, Boston University School of Medicine, Boston, MA 02118, USA
[6]These authors contributed equally
[7]Lead Contact
*Correspondence: cbrangwy@princeton.edu
https://doi.org/10.1016/j.cell.2020.03.050

SUMMARY

Liquid-liquid phase separation (LLPS) mediates formation of membraneless condensates such as those associated with RNA processing, but the rules that dictate their assembly, substructure, and coexistence with other liquid-like compartments remain elusive. Here, we address the biophysical mechanism of this multiphase organization using quantitative reconstitution of cytoplasmic stress granules (SGs) with attached P-bodies in human cells. Protein-interaction networks can be viewed as interconnected complexes (nodes) of RNA-binding domains (RBDs), whose integrated RNA-binding capacity determines whether LLPS occurs upon RNA influx. Surprisingly, both RBD-RNA specificity and disordered segments of key proteins are non-essential, but modulate multiphase condensation. Instead, stoichiometry-dependent competition between protein networks for connecting nodes determines SG and P-body composition and miscibility, while competitive binding of unconnected proteins disengages networks and prevents LLPS. Inspired by patchy colloid theory, we propose a general framework by which competing networks give rise to compositionally specific and tunable condensates, while relative linkage between nodes underlies multiphase organization.

INTRODUCTION

Eukaryotic cells coordinate their biochemical reactions using organelles. In addition to traditional membrane-enclosed organelles, cells feature a vast array of membraneless compartments, which exhibit substructure and form interfaces with each other. Unlike those of the nucleus (e.g., nucleoli, speckles) (Mao et al., 2011; Nizami et al., 2010; Zhu and Brangwynne, 2015), membraneless organelles in the cytosol typically form in a context-dependent manner as a consequence of altered RNA homeostasis (stress granules, SGs; P-bodies, PBs) (Ivanov et al., 2019; Protter and Parker, 2016; Youn et al., 2019) or extracellular cues (signalosomes) (Gammons and Bienz, 2018; Schaefer and Peifer, 2019; Wu and Fuxreiter, 2016). Recent studies suggest that the physics of liquid-liquid phase separation (LLPS) dictate the formation of these droplet-like structures (Brangwynne et al., 2009; Li et al., 2012), which are increasingly referred to as condensates (Banani et al., 2017; Shin and Brangwynne, 2017). However, despite a flurry of recent attention, the molecular rules that account for their unique protein and nucleic acid compositions and "multiphase" patterning remain elusive.

Similarities between proteins essential for assembly of diverse condensates may inform the molecular origins of their formation and compositional specificity. Many of these proteins feature a modular organization with a structured self-oligomerization domain (OD), intrinsically disordered region (IDR), and substrate-binding moiety (Mitrea and Kriwacki, 2016; Figure 1A). In the case of RNA-dependent condensates, essential proteins feature an RNA-binding domain (RBD) with a folded, sequence-specific region (e.g., RNA recognition motif [RRM]) and/or a promiscuous, low-affinity arginine-rich motif (e.g., Arg-Gly-Gly [RGG], Ser-Arg [SR]) (Chong et al., 2018; Mitrea et al., 2016; Thandapani et al., 2013). In principle, compositional specificity might be encoded by unique RBD-RNA interactions combined with stable self-oligomerization or additive weakly interacting IDR stickers ("self-associating IDRs"), both of which are sufficient for LLPS *in vitro* (Feric et al., 2016; Frey et al., 2006; Kato et al., 2012; Mitrea et al., 2016; Molliex et al., 2015; Nott et al., 2015; Patel et al., 2015). Whether this is the case for the vastly more complex condensates of the crowded intracellular environment is unclear, particularly given that many RBDs (e.g., RGG) and self-associating IDRs lack strong substrate discriminatory abilities.

SGs (Kedersha et al., 1999) are an ideal prototype for dissecting general mechanisms of intracellular LLPS, including that of

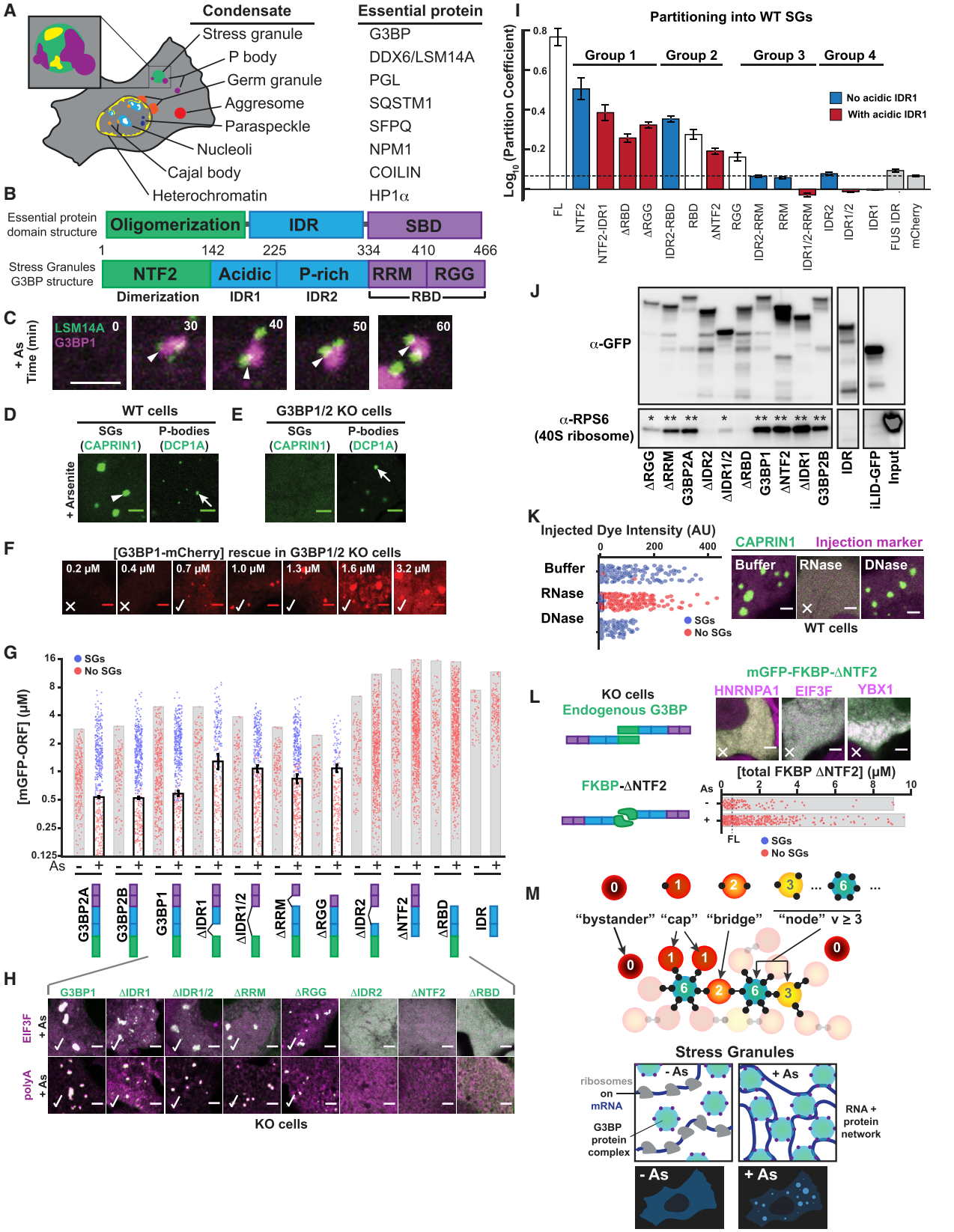

(legend on next page)

specificity, as they feature multiphase structure, are not required for cell viability, form in a controllable manner, and have known composition (Ivanov et al., 2019; Protter and Parker, 2016; Youn et al., 2019). These micron-sized RNA-protein droplets form in mammalian cells upon translational arrest and subsequent polysome disassembly, which releases exposed RNA into the cytoplasm (“RNA influx”) (Boeynaems et al., 2017; Kedersha et al., 1999, 2002, 2016; Kroschwald et al., 2015; Molliex et al., 2015; Wheeler et al., 2016; Wippich et al., 2013). Despite largely liquid-like dynamics, SGs may exhibit a less dynamic substructure (Jain et al., 2016; Niewidok et al., 2018; Souquere et al., 2009) and are frequently attached to the compositionally related PBs (Eystathioy et al., 2002, 2003; Kedersha et al., 2005; Moon et al., 2019; Tauber et al., 2020). Despite this patterning and the known involvement of a complex network of RNA-binding proteins (RBPs) (Markmiller et al., 2018; Youn et al., 2018), studies indicate the essentiality of a single protein, G3BP, for RNA-dependent SG condensation (Guillén-Boixet et al., 2020 [this issue of *Cell*]; Bley et al., 2015; Kedersha et al., 2016; Matsuki et al., 2013; Yang et al., 2020 [this issue of *Cell*]; Tourrière et al., 2003). Although it features the modular architecture described above (Figure 1B), why G3BP is important for SG biogenesis relative to other abundant RBPs, and the mechanisms by which compositional specificity and multiphase coexistence of SGs/PBs are encoded, remain to be determined.

Here, we use quantitative live cell reconstitution and biochemical assays, along with network concepts from graph theory and the study of “patchy” colloids, to dissect the relative contributions of oligomerization, RNA binding, and protein disorder in multiphase SG/PB condensation. We show that the constitutive G3BP dimer, as well as its high-affinity binding partner UBAP2L, serve as interaction nodes to collectively confer the high number of RNA-binding contacts (RBD “valence”) needed to form a condensed ribonucleoprotein (RNP) network following RNA influx. Binding partners that lack RBDs act as “valence caps” on the G3BP node, disengaging its protein-protein interaction (PPI) network, thus decreasing RNA-binding capacity and abrogating SG assembly. We show that G3BP’s IDRs do not self-interact but rather modulate RNA binding via relative juxtaposition of a repulsive acidic region (see also accompanying papers Guillén-Boixet et al., 2020 and Yang et al., 2020). Differentiation between PBs and SGs is context dependent, as changes in node stoichiometry create unique condensates that do not conform to any one description of a canonical RNP body. We propose that similar competing protein interaction networks are a ubiquitous mechanism by which cells spatiotemporally modulate multiphase coexistence and associated substrate processing.

RESULTS

G3BP Dimerization and RNA Binding Are Necessary but Not Sufficient for Stress Granule Formation

To elucidate the molecular rules of SG assembly and multiphase coexistence with PBs (Figure 1A), we began by examining the minimal components required for SG assembly. In wild-type (WT) human U2OS cells, arsenite (As) treatment (400 μM, 1 h) causes the formation of PB-attached SGs (Figure 1C). Conversely, G3BP1 and G3BP2 (G3BP1/2) double knockout (G3BP KO) cells do not exhibit As-induced SGs, but form PBs (Figures 1D, 1E, S1A, and S1B; Kedersha et al., 2005, 2016). A concentration threshold characterizes systems that undergo LLPS (Boeynaems et al., 2018; Brangwynne et al., 2015), raising the question of whether this is valid for G3BP-mediated SGs. Live cell microscopy reveals that G3BP KO cells stably expressing ectopic G3BP at low concentrations (0–0.6 μM) never exhibit microscopically detectable SGs following As treatment, but upon exceeding ~0.6 μM, SGs become observable in nearly all cells (Figures 1F and S1A–S1E). No G3BP isoform causes SG assembly in the absence of stress, and micro-injection of RNase prevents their formation (Figure 1K), both of which are consistent with an essential role for RNA influx (Bounedjah et al., 2014).

Figure 1. G3BP Dimerization and RNA Binding Are Necessary but Not Sufficient for Stress Granule Formation

(A) Essential proteins for condensates. Inset: P-bodies (PBs, purple) attach to stress granules (SGs, green) with substructure (yellow).

(B) Top: Essential protein domain organization (IDR = intrinsically disordered region, SBD = substrate-binding domain). Bottom: G3BP SBD = RNA-binding domain (RBD), with Arg-Gly-Gly (RGG) region and RNA recognition motif (RRM).

(C) U2OS cells treated with 400 μM arsenite (As) form SGs with attached PBs. Lentivirus-based stable protein expression used in all experiments. Unless noted: scale bar, 3 μm.

(D) Wild-type (WT) cells (+As) with GFP-CAPRIN1 (SGs, arrowhead) or GFP-DCP1A (PBs, arrow).

(E) Same as (D) but G3BP1/2 double KO (“G3BP KO”) cells.

(F) Dose-response of SG rescue (yes = check, no = X) by G3BP1-mCherry (mCh) in G3BP KO cells (+As).

(G) Quantification of GFP-G3BP concentration threshold for SGs in KO cells (EIF3F-mCh co-positivity, +/− As). Mean and SEM: n = 4 experiments, 4 images per. All experiments: each dot = one cell analyzed.

(H) Top: representative images for (G). Bottom: KO cells (+As) with GFP-G3BP1 deletions (Δs) were fixed followed by oligo-dT RNA-FISH to detect polyA+ mRNA (magenta) and SGs (check).

(I) WT U2OS cells with CAPRIN1-GFP and mCh-tagged protein. SG partition coefficient (PC) mean and SEM: n = 3 experiments (n > 4 images per). Dashed line = PC of mCh control.

(J) GFP-G3BP1 Δs were immunoprecipitated (IPed) from KO U2OS cells (-As) with anti (α)-GFP (then RNase and RIPA-wash) to isolate tightly bound 40S ribosomes (* = low, ** = high RPS6). Representative blot (n = 3 experiments).

(K) WT U2OS cells with GFP-CAPRIN1 were injected with buffer, RNase, or DNase, and As-treated; then SGs were assessed (n = 3 experiments, > 100 cells per).

(L) G3BP KO cells (+As) with mCh SG proteins and GFP-FKBP-G3BP1ΔNTF2. Dashed line = rescue threshold for WT G3BP1. Images: ~8 μM GFP. X = no SGs.

(M) Top: graph theory framework for network-based condensation. “Valence” (v) = “particle” (protein or protein complex) interaction sites: $v = 0$ (bystander), $v = 1$ (cap); $v = 2$ (bridge), $v > 2$ (node). Bottom: exposed RNA for G3BP complex-binding is low; following As, RNA is exposed (ribosomes disassemble), and condensation occurs if RNA-binding v of G3BP node is sufficiently high.

See also Figure S1.

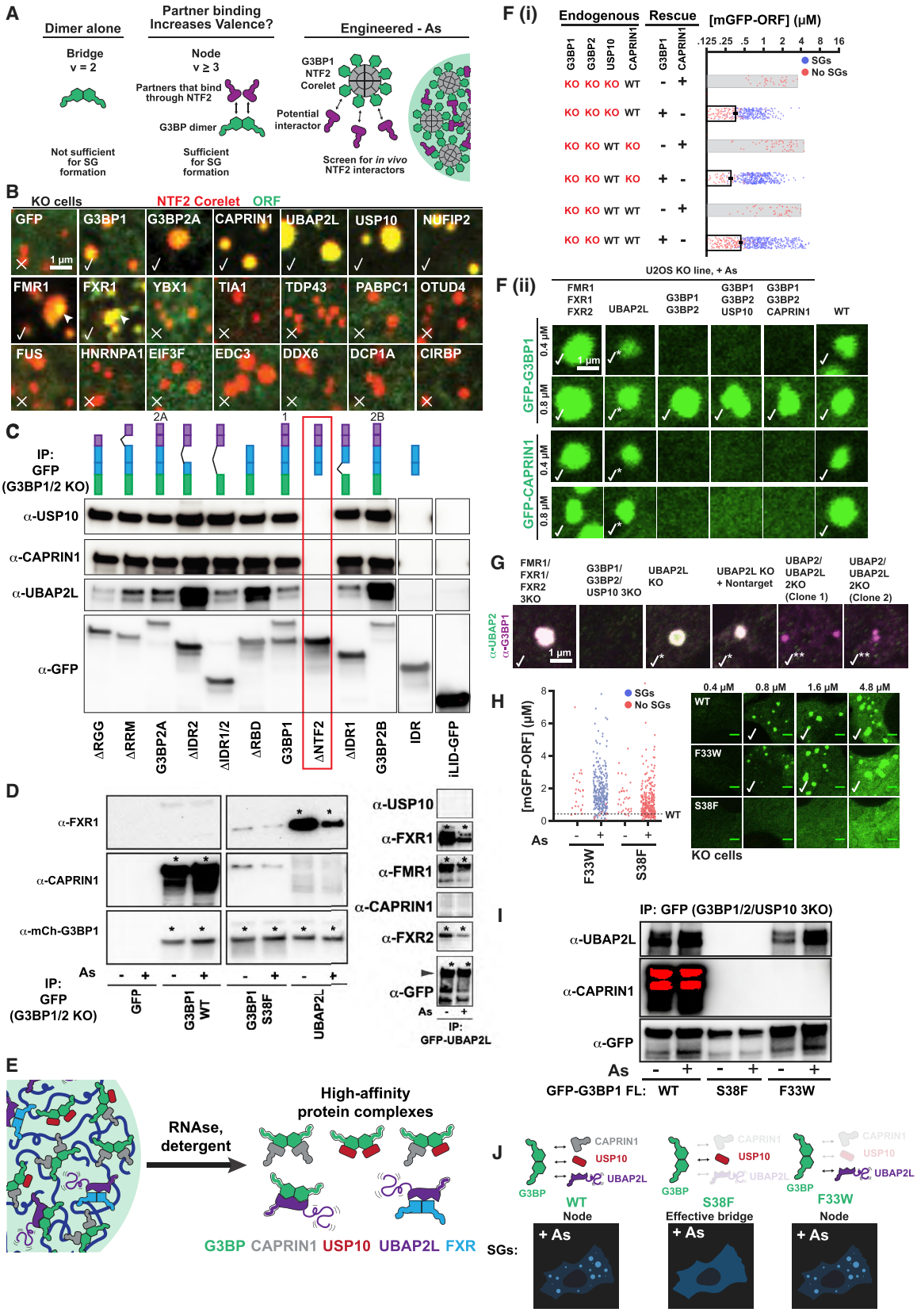

(legend on next page)

Studies show that G3BP is dimeric, as is its isolated NTF2-like domain (hereafter, NTF2) (Figures 1B and 2D; Guillén-Boixet et al., 2020; Kedersha et al., 2016; Kristensen, 2015; Panas et al., 2015; Yang et al., 2020; Tourrière et al., 2003; Vognsen et al., 2013). To examine the necessity of individual G3BP regions, we expressed a series of deletion constructs, determining concentration thresholds for SG formation (+/− As). Both dimerization and RNA binding (via RRM or RGG) are essential for G3BP's central role in SG assembly, as SGs form in As-treated cells expressing ΔRRM or ΔRGG, but not ΔRBD (both RRM and RGG are deleted) or ΔNTF2 (no dimers) (Figures 1G, 1H, and S1F–S1I). However, for ΔRGG, SGs are smaller and the threshold for rescue is higher, which may account for divergence from previous studies (Bley et al., 2015; Kedersha et al., 2016; Matsuki et al., 2013). The requirement for the NTF2 and RBD correlates with their ability to partition into SGs in WT cells (Figure 1I), which reflects interaction preference for RNPs in the SG network relative to the bulk cytoplasm.

Self-associating IDRs are implicated as key drivers of LLPS (Ruff et al., 2019) and potentially SG formation (Fang et al., 2019; Molliex et al., 2015; Patel et al., 2015). However, for G3BP, removal of either acidic IDR1 or both IDR1 and IDR2 (IDR1/2) causes only a minor shift in its threshold for LLPS (Figure 1G). Surprisingly, unlike ΔIDR1/2, deletion of just the proline-rich IDR2 blocks rescue of SG defects, suggesting a modulatory role for relative domain juxtaposition. As both IDR1 and IDR2 fail to partition into SGs, while presence of acidic IDR1 decreases partitioning of diverse fragments (Figure 1I), we hypothesized that its high negative charge causes electrostatic repulsion of RNA, the most abundant biomolecular component in SGs (Bounedjah et al., 2014). Consistent with this, ΔIDR2 and ΔRBD similarly lack the ability to bind rRNA-rich 40S ribosomes (Figure 1J).

Our findings underscore the importance of G3BP dimerization and RNA binding in SG condensation. A simple physical picture is that RBD dimers "cross-link" exposed RNA following polysome disassembly. To test this, we replaced G3BP's NTF2 with synthetic light-activated (iLID- and sspB- [iLID/sspB]) (Guntas et al., 2015) or constitutive (FKBP) (Rollins et al., 2000) dimerization domains. Unexpectedly, stable expression of either full-length (FL) G3BP dimer mimetic failed to rescue SGs at concentrations greatly exceeding physiological values (Figures 1L and S1J). In parallel, we transiently expressed iLID/sspB-ΔNTF2 using Lipofectamine. In cells with both components at far higher concentrations than achieved with tolerated stable expression, SGs are observed (Figure S1J). This concentration threshold (20 μM) is > 30× that of FL G3BP (0.6 μM) (Figures 1G, S1D, and S1J). We cannot rule out the possibility that high levels of plasmid-encoded mRNA and cationic Lipofectamine, which can induce interferon signaling and SG assembly in WT cells, contribute to this effect (Guo et al., 2019; Hagen et al., 2015; Panas et al., 2019; Tourrière et al., 2003). Thus, NTF2-mediated dimerization of the RBD is necessary, but not sufficient, for SG formation at physiological G3BP concentrations (~1.8 μM in HeLa cytoplasm, Hein et al., 2015); ~2.2 μM in U2OS, see Quantification and Statistical Analysis).

Stress Granule Condensation Requires G3BP-UBAP2L Complexes

From work with patchy colloids (Bianchi et al., 2011), a system of interacting particles can only phase separate into a dynamically connected network if each particle has a sufficient number of sites to engage other particles, which defines its valence, *v* (Figure 1M); here, the "particle" (or "vertex" in graph theory) represents an individual protein, RNA, or stable complex. Generally speaking, $v>2$ are essential, with higher valences more readily driving LLPS. In the case of synthetic G3BP dimers (Figure 1L), there are only two interaction interfaces, and they thus feature overall $v=2$ (two RBD-RNA interfaces); we refer to $v=2$ particles as "bridges," which might contribute to phase separation by linking higher-valence particles, but cannot on their own form a space-spanning interaction network (Figure 1M).

Given that a generic dimerization domain cannot replace G3BP's NTF2, we reasoned that rather than a bridge ($v=2$), the G3BP dimer embodies a particle of $v\geq3$; we refer to such objects as "nodes" (Figure 1M). In the case of an endogenous G3BP dimer, such valence would be achieved by at least one heterotypic PPI with the NTF2 domains, in addition to the two RBDs. If so, NTF2 might serve as an interaction platform for additional RNA-binding nodes and amplify the overall valence—and hence RNA-binding capacity—of the resulting complex (Figure 2A). To screen for such SG proteins, we harnessed NTF2's dimerization abilities in the context of a

Figure 2. Stress Granule Condensation Requires G3BP-UBAP2L Complexes

(A) Dimeric G3BP RBD bridges ($v=2$) are not sufficient for SGs; G3BP must act as node ($v>2$) via additional high-affinity protein-protein interactions (PPIs) with its NTF2 dimerization domain; right: live cell Corelet assay to screen for PPIs.

(B) G3BP KO cells (No As) with G3BP NTF2 Corelets (red, sspB-mCh-G3BP1ΔRBD; no tag, iLID-Fe core) and GFP-tagged proteins (10-min activation). Checks = putative NTF2 partners/PPIs.

(C) GFP-G3BP1Δs IPed from G3BP KO cells (No As) with α-GFP (then RNase and RIPA-wash) to isolate tightly bound proteins. ΔNTF2 (red box) abolishes binding. Representative blot (n = 3 experiments).

(D) GFP-tagged proteins IPed similar to (C), but ± As. Representative blot (n = 3 experiments), * = high-affinity interaction.

(E) High-affinity, RNA-independent complexes predicted by IPs.

(F) Top (i): Quantification of GFP-G3BP concentration threshold for SGs in KO cells (+As). Mean and SEM: n = 3 experiments (n > 4 images per). Bottom (ii): KO cells with GFP-tagged protein at indicated concentration, check = SGs, check* = smaller SGs.

(G) Panel of U2OS KO cells (+As) examined for SGs by immunofluorescence. Indicated: no SG defect (check), smaller SGs (check*), very small SGs in rare cells (check**).

(H) Quantification of G3BP variant concentration threshold for SGs in G3BP KO cells (+/− As). Mean and SEM: n = 3 experiments (>4 images per). Representative images at indicated concentrations (+As, check = SGs).

(I) GFP-G3BP variants IPed similar to (D), but in G3BP1/2/USP10 3KO cells. Representative blot (n = 3 experiments).

(J) G3BP variants form complexes of different valence, which corresponds to ability to rescue SG defects.

See also Figure S2.

two-component optogenetic biotechnology known as Corelets (Bracha et al., 2018). Corelets are comprised of a 24-mer ferritin "core" coated by iLID molecules, which acts as an oligomerization platform following blue light-stimulated sspB-iLID interactions (Bracha et al., 2018). By changing the relative concentration of the two components, the oligomerization state (valence) can be varied (0 to 24) and intracellular phase diagrams can be mapped (Bracha et al., 2018). We hypothesized that NTF2 dimers would form homotypic links between cores and cause condensation, allowing microscopy-based identification of heterotypic NTF2-interacting partners by their relative partitioning (Figure 2A). In a panel of abundant (Table S1) and frequently studied GFP-tagged SG (n = 20) and PB (n = 3) proteins, only eight SG proteins (USP10, UBAP2L, CAPRIN1, FMR1, FXR1, NUFIP2, G3BP1, and G3BP2A) partition strongly into NTF2 condensates (G3BPΔRBD Corelets) (Figure 2B). These proteins are specific to NTF2 interactions, as they are not observed in a non-SG Corelet condensate (FUS IDR) (Figure S2A). To validate these proposed NTF2-binding partners, we performed biochemical studies, finding that G3BP-mediated co-immunoprecipitation ("co-IP") of USP10, CAPRIN1, and UBAP2L all require its NTF2 domain; as interactions are preserved following RNase and stringent washing, we refer to these as "high affinity" (Figure 2C). Conversely, FMR1 and FXR1, which assemble into dimers (Adinolfi et al., 2003; Dolzhanskaya et al., 2006), co-IP with UBAP2L, but not G3BP and CAPRIN1, allowing us to infer the existence of distinct high-affinity protein complexes (Figures 2D and 2E).

We reasoned that the identified proteins might serve as G3BP-interacting bridges or nodes to contribute additional, essential RNA-binding interfaces (valence) for condensing the SG RNP network; we note that all but USP10 have RBDs. To investigate this, we generated a series of single- and multi-KO U2OS cell lines. KO of USP10, CAPRIN1, NUFIP2, FXR1/FXR2/FMR1 (3KO), or FXR1/FXR2/FMR1/NUFIP2 (4KO) had no effect on SG formation (Figures 2F and 2G). USP10 and CAPRIN1 are unlikely to play major roles in SG condensation at endogenous levels in U2OS cells, as associated G3BP 3KOs (G3BP1/G3BP2/USP10, G3BP1/G3BP2/CAPRIN1) require similar concentrations of G3BP for rescue relative to 2KO (Figure 2F). In contrast, UBAP2/2L 2KO results in smaller SGs, which form in only a minority of cells (Figure 2G), a finding supported by others (Cirillo et al., 2020; Huang et al., 2020; Markmiller et al., 2018; Yang et al., 2020; Youn et al., 2018). Since UBAP2/2L 2KO has no effect on CAPRIN1 and G3BP1 levels and only slightly reduces USP10 and G3BP2 (Figure S2E), these data suggest that UBAP2/2L (hereafter, paralogs referred to as "UBAP2L") might act as a critical G3BP-associated node. In strong support of this hypothesis, we serendipitously discovered a missense mutation in G3BP's NTF2 domain (S38F), which blocks its ability to rescue SG formation (Figure 2H). G3BP S38F forms dimers (Figures 2D and S2D), binds USP10 (Figure S2C), and partitions strongly into SGs when expressed with WT G3BP (Figure S2B). However, the S38F variant is unable to form high-affinity complexes with CAPRIN1 or UBAP2L (Figure 2I), suggesting that the mutation changes G3BP from a $v \geq 3$ node to a $v=2$ bridge, which no longer engages required valence from UBAP2L. Importantly, a previously identified G3BP NTF2 variant (F33W) (Kedersha et al., 2016) retains association with UBAP2L, but not USP10 or CAPRIN1 (Figure 2I), yet displays a similar threshold concentration for rescue as WT (Figure 2H). Taken together, these data provide compelling support for G3BP-UBAP2L complexes playing an essential role in SG condensation by virtue of their node identities (Figure 2J).

Valence Capping of the G3BP Node by RBD-Lacking Binding Partners Prevents Stress Granule Formation

Having identified NTF2-interacting proteins that may contribute RBD valence to the G3BP complex, we turned to investigate the role of USP10, the only identified partner without an RBD. We hypothesized that USP10 competes with RBPs (e.g., UBAP2L) for NTF2 binding and effectively "caps" the G3BP node; reduction of the overall valence of the complex would disrupt the formation of a space-spanning network (Figure 3A). To test this "valence capping" model, we examined the effect of USP10 concentration on G3BP-dependent SG formation. Building on qualitative studies (Kedersha et al., 2016; Panas et al., 2015), competitive inhibition experiments in G3BP KO cells indicate that USP10 impacts the G3BP rescue threshold as a function of stoichiometry, with a slope of ~1 (i.e., cells require excess G3BP relative to USP10 to form SGs) (Figures 3B, 3C, and S3F). This is consistent with G3BP monomer binding a single USP10 molecule, which disengages other RBPs from its NTF2 interface. Expression of USP10's NTF2-interaction motif ("NIM," amino acids 1–33) results in identical inhibition (slope~1) (Figures 3B, S3B, and S3C), indicating that FL USP10 does not act as a bridge between G3BP and other SG components. A panel of controls (n = 15 proteins) demonstrates specificity of inhibition to USP10 (Figure S3A), and optogenetic approaches support an NTF2-dependent mechanism of action (Figures S3D and S3E).

Previous work speculated that differential USP10 versus CAPRIN1 binding toggle G3BP between conformations that inhibit or promote RNP condensation (Kedersha et al., 2016). In contrast, our valence capping model proposes that USP10 acts as a $v=1$ interactor ("cap") that decreases the overall valence of the G3BP complex. This hypothesis makes a specific and testable prediction: NTF2-binding bridges and nodes ($v \geq 2$) will similarly inhibit SG formation if their RBDs are removed, such that they too become caps ($v=1$) (Figure 1M). Informed by G3BP interaction domain-mapping studies (Baumgartner et al., 2013; Solomon et al., 2007; Youn et al., 2018), we generated GFP-tagged CAPRIN1 and UBAP2L caps (NIM only, $v=1$), bridges (NIM and RBD, $v=2$), and bystanders (lacks NIM, $v=0$), and performed competitive inhibition experiments in G3BP KO cells. Predicted bridges and bystanders have no effect on G3BP rescue (slope~0), whereas both CAPRIN1 and UBAP2L caps inhibit (positive slope) (Figures 3D, 3G, and S3B). The UBAP2L NIM cap is a less potent inhibitor than that of USP10 or CAPRIN1, which agrees with co-IP studies assessing relative binding of the FL proteins to G3BP (Figure 2C) and illustrates that degree of valence capping is dependent on relative interaction strengths (Figure 3A).

Although disfavored by prior work (Panas et al., 2015, 2014; Schulte et al., 2016), an alternative explanation is that USP10 disrupts NTF2 dimers. To test this, we generated a USP10 NIM doublet to change it from a cap ($v=1$) to a bridge ($v=2$, "NIMx2"), reasoning that if NIM disrupts G3BP dimers, NIMx2

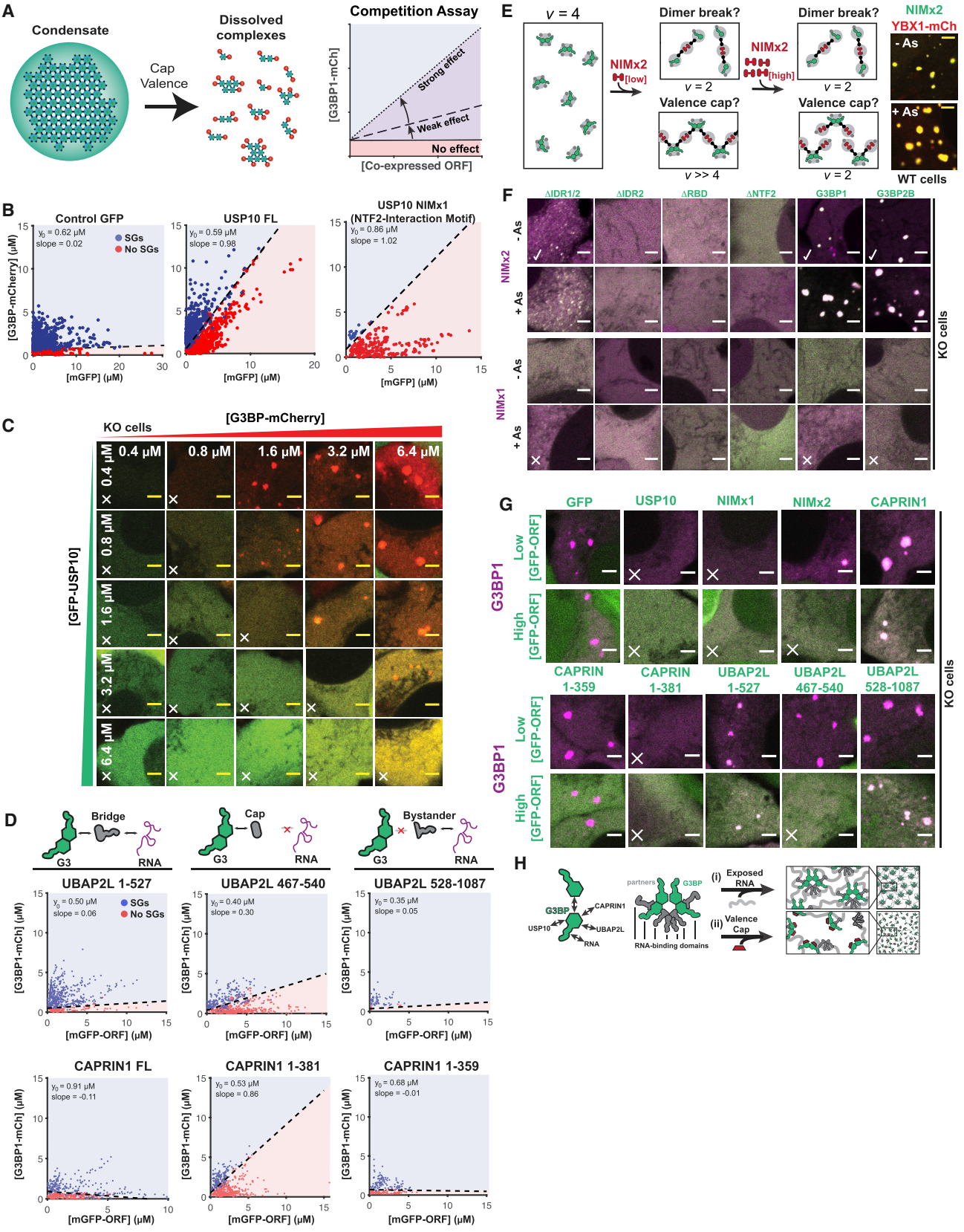

(legend on next page)

would link two G3BP monomers into a complex with insufficient valence (v=2) for condensation (Figure 3E). Inconsistent with this model, expression of NIMx2 in WT cells causes formation of granules in the absence of stress (Figure 3E). Examination of KO cells (+/− As) co-expressing NIMx2 and G3BP deletions revealed that both NTF2 and RNA binding are required (Figures 3F and 3G), which signifies a requisite amplification of RNA-binding valence. Strikingly, NIMx2 displays "reentrant" properties, promoting SG formation at low ratios relative to G3BP and inhibiting at high (>3) (Figures 3E–3G and S3B). This reentrant phase transition likely results from a lack of available NIM-free G3BP for polymerization (Figure 3E) and can be recapitulated using an engineered system (Figure S3G). Taken together, these data negate the possibility that USP10 disrupts G3BP dimers, but instead favors a valence-capping model (Figure 3H).

High Valence G3BP RBD Nodes Are Sufficient for Stress Granule Formation with Attached P-Bodies

Our data suggest that highly multivalent RNA-binding complexes are necessary for SG condensation, but a stringent test of this model requires experimental control of RBD valence (v_{RBD}). To quantitatively interrogate the relationship between v_{RBD}, protein complex concentration, and RNA availability, we again utilized the optogenetic Corelet system (Bracha et al., 2018). Replacing the dimerization domain (NTF2) of G3BP with sspB ("ΔNTF2 Corelets") (Figure 4A), we find that non-stressed G3BP KO cells require a very high degree of RBD oligomerization (v_{RBD} ~24 at 0.15 μM Core) for LLPS (Figures 4F and 4G). Following As treatment (stress), LLPS occurs at lower core concentrations and valences (v_{RBD} ~8 at 0.15 μM Core), and the resulting granules are larger (Figures 4F and 4G). Stress-dependent LLPS occurs rapidly (seconds) and is reversible (Figures 4B and S4A), indicating that multivalent RNA-binding contacts are essential for both SG formation and maintenance. Such condensates mimic the properties of endogenous SGs, including a dependence on RNA influx (Figures 4E–4H, S4F, and S4G), recruitment of SG proteins and polyA+ mRNA with attachment of PBs (Figure 4J), and liquid-like dynamics (Figures 4C and 4D). We therefore refer to these structures as optogenetic SGs (opto-SGs).

The shift in the ΔNTF2 Corelet phase threshold after RNA influx can be visualized in As-treated cells subjected to repeated cycles of activation and deactivation, which triggers valence-dependent opto-SG assembly on a timescale similar to endogenous SGs (Figures 4H and S4F). Such a shift is negated by pretreatment with cycloheximide, which blocks polysome disassembly and RNA influx (Figures 4E–4G and S4G), and long-term inhibition of RNA transcription by Actinomycin D prevents opto-SG formation (Figures 4F and 4G). We emphasize that these drug-dependent changes in LLPS are not Corelet artifacts: similar threshold shifts are absent for self-associating FUS IDR Corelet condensates (Figures S4D and S4E), which do not recruit SG proteins (Figure S2A) and are thus not SGs; this is consistent with previous studies using an orthogonal Cry2-based opto-Droplet approach (Shin et al., 2017; Zhang et al., 2019).

To determine the minimal G3BP domain for opto-SG LLPS, we examined ΔNTF2 Corelets with additional regions deleted. Consistent with a lack of SG partitioning (Figure 1I), G3BP's central IDRs do not self-interact, as IDR1, IDR2, and IDR1/2 Corelets never cause LLPS (+/− As) (Figures S4H–S4K). In contrast, both G3BP RBD (RRM and RGG) and IDR2-RBD Corelets form polyA+ opto-SGs containing all tested SG proteins (Figures 4I, 4J, S4B, and S4C). Underscoring its utility as a biotechnology, G3BP Corelets replicate several phenotypes of corresponding GFP-tagged deletions. First, ΔNTF2/ΔIDR2 (synthetic GFP-G3BPΔIDR2) fails to form granules (+/− As) (Figure 4I). Second, similar to GFP-ΔIDR1, ΔNTF2/ΔIDR1 forms irregular granules (Figures 4I and S4C). Third, RBD-only Corelets feature a right shifted phase threshold relative to ΔNTF2 (Figure 4I). Finally, all such condensates are reversible, form multiphase structures with PBs, and similarly recruit SG proteins and polyA+ RNA (Figures 4J, S4B, and S4C). Thus, Corelets recapitulate nearly all features of GFP-based rescue experiments (see also Figures S4J and S4K) and represent a powerful synthetic approach for assessing the relationship between RBD valence, RBD identity, and SG/PB composition and coexistence.

Stress Granules with Attached P-Bodies Are the Default Multiphase Condensate Encoded by High Valence RBD Nodes

Unlike synthetic dimers, highly multivalent G3BP RBD Corelets are sufficient to compensate for FL G3BP and assemble SGs. Given that G3BP is a constitutive RBD dimer, this finding is only biologically meaningful if interaction partners contribute additional RBD valence (v_{RBD}) to the protein complex. If true, we reasoned that such G3BP NTF2-associated proteins would act similarly upon oligomerization of their RBDs, forming compositionally identical SGs that adhere to PBs (Figure 5A). To test this, we mapped phase diagrams for UBAP2L and CAPRIN1

Figure 3. Valence Capping of the G3BP Node by RBD-Lacking Binding Partners Prevents Stress Granule Formation

(A) Interacting "caps" (v = 1) are proposed to disrupt networks of high v particles. Right: SG rescue competition assay (G3BP KO cells) tests model by co-expressing GFP-tagged NTF2 partners (cap, positive slope) with G3BP1-mCh.

(B) Competition assay for predicted caps in G3BP KO cells (+As). Indicated: y-intercept (G3BP rescue concentration, no competitor), best-fit slope demarcating ± SG cells.

(C) Representative images for (B, middle) at indicated protein concentrations (X, no SGs).

(D) Competition assay similar to (B) with CAPRIN1/UBAP2LΔs.

(E) NTF2-interacting motifs (NIMs) inhibit SGs by "dimer breaking" or "valence capping," differentiable using a v = 2 NIM bridge ("NIMx2"). If capping: low NIMx2 promotes condensation, polymerizing G3BP dimers (high v_{RBD}); high, inhibits by saturation (v_{RBD} = 2). If breaking, low and high NIMx2 link G3BP monomers (v_{RBD} = 2). Right: GFP-NIMx2 induces SGs in WT U2OS (-As).

(F) Representative images (X, inhibits SGs; check, promotes): G3BP KO cells (+/− As) expressing GFP-G3BPΔs and mCh-NIMx1 (or x2)

(G) Images (X, inhibits SGs) for G3BP KO cells (+As) with mCh-G3BP1 and GFP-tagged protein (low or high levels).

(H) Molecular model for SG regulation by NTF2 PPIs.

See also Figure S3.

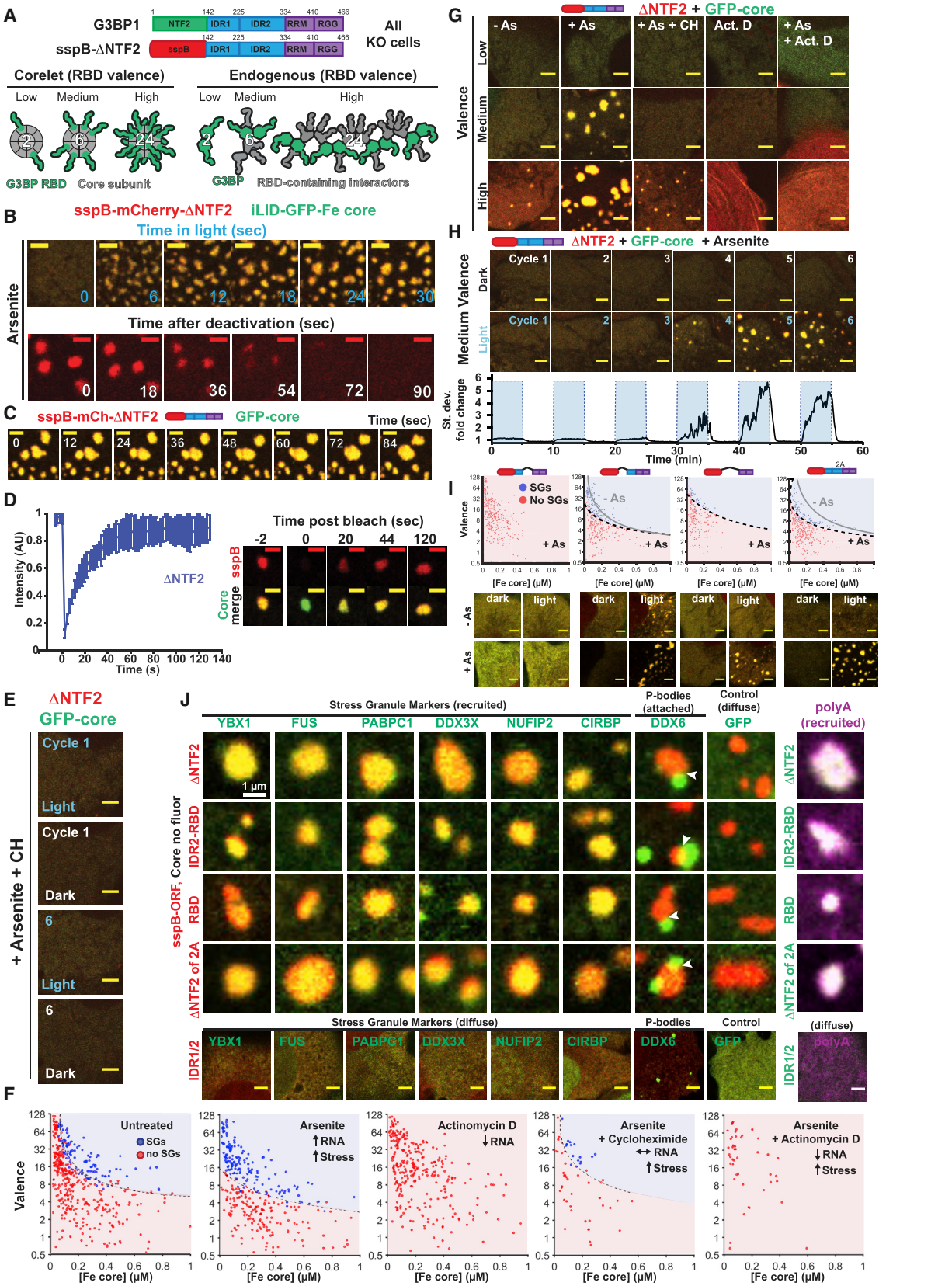

(legend on next page)

RBD Corelets (G3BP KO, +/− As) (Figures 5B and 5C). Surprisingly, despite each featuring a single RGG, both RBDs are even more potent than G3BP RBD (1 RRM, 1 RGG) at enabling SG formation in both the Corelet system (Figure 5C) and when placed into GFP-G3BP chimeric proteins (Figures 5E and S5J). Similar to G3BP RBD Corelets, As-induced RNA influx causes a shift in their associated phase thresholds and results in reversible, PB-studded opto-SGs with all tested markers (Figures 5C, 5D, and S5). However, both As-induced threshold shifts are minor relative to G3BP RBD (Figure 4F), which could potentially arise from self-interactions that contribute to LLPS. We refuted this possibility, as RNA depletion inhibits CAPRIN1 RBD LLPS (Figure S5A), as does scrambling its sequence (Figure S5C). We thus infer that NTF2-associated RBPs are indeed capable of contributing v_{RBD} to the multi-protein G3BP complex.

It is conceivable that multivalent NTF2-associated RBDs are unique in engaging SG RNPs to form a condensed network that coexists with that of PBs. However, the RBD of FXR1, a dimeric RBP that interacts with UBAP2L but not NTF2 (Figure 2D), mimics G3BP RBD in all assays (Figures 5B–5E and S5E–S5J). Remarkably, use of a large panel of additional Corelets (n = 25) indicates that high v_{RBD} is sufficient for PB-studded, polyA+ SG assembly, irrespective of whether the RBD is folded (RRM) or unfolded (RGG), from an SG or PB protein, or linked to G3BP IDR (Figures 5F–5I and S5E–S5G). Despite this RBD interchangeability, we surmise that RBD-RNA specificity and relative interaction strengths contribute to the lack of relationship between type and number of RNA-binding motifs and relative phase thresholds (Figures 5C and 5F–5H). Importantly, Corelets are capable of plugging into non-SG interaction networks, as those of DCP1A—a PB protein with PPIs but no RBD—recruit PB but not SG markers (Figure 5J). Thus, polyA+ SGs with attached PBs are the "default" multiphase condensate encoded by high-valence RBD nodes (Figure 5K).

A Self-Associating IDR in UBAP2L Is Critical to Its Ability to Act as a Valence-Multiplying Node

Unlike other proteins, mild expression (<1 μM) of UBAP2L or FXR1 rescues SG defects in G3BP KO cells (Figures 6A, 6B, and S6A–S6C), implying that they can act as G3BP-independent SG nodes. We hypothesized that, in each of these cases, a self-associating domain would confer the requisite valence for node identity ($v \geq 3$). Although previous studies have indicated that such a domain (dimerization) exists for FXR1 (Adinolfi et al., 2003; Dolzhanskaya et al., 2006), one has yet to be described for UBAP2L. Using a Corelet screen for PPI valence (n = 13 UBAP2L/CAPRIN1 fragments) (Figure 6C), we identified a non-dimeric (Figure 6H), self-associating IDR in UBAP2L (781–1087), which is essential for its ability to rescue SG defects in G3BP KO cells (Figures 6C, 6D, and S6D–S6G). We surmise that this "sticky" IDR facilitates weak interactions between UBAP2L proteins in separate high-affinity complexes (FXR1/UBAP2L, UBAP2L/G3BP), thus acting as an essential valence multiplier for SG formation (Figure 6E).

Competition between Protein-Protein Interaction Nodes Encodes Multiphase Condensation

Consistent with previous studies (Cirillo et al., 2020; Jain et al., 2016; Niewidok et al., 2018), super-resolution live cell microscopy revealed the presence of micro-phases ("cores") within SGs (Figure 6G), which could provide insight into the rules governing phase miscibility. Since high-affinity UBAP2L complexes containing both FXR1 and G3BP are undetectable (Figure 2D), we hypothesized that the two dimeric nodes compete for available UBAP2L, with their relative stoichiometry critical for the observed mixed distribution in SGs by conventional confocal microscopy. Indeed, unlike UBAP2L, high ratios of FXR1 to G3BP cause demixing within SGs, as detected by G3BP-enriched and -depleted regions in individual granules (Figures 6F and S7A–S7C).

We reasoned that node stoichiometry similarly impacts SG/PB coexistence. In agreement with this, overexpression of UBAP2L in G3BP KO cells causes the formation of condensates that are not canonical SGs or PBs, containing common markers of both (Figures 6H, S6A–S6C, and S6H–S6J). The collapse of many SG and PB components into a single miscible phase may result from UBAP2L's high-affinity interaction with the essential PB node, DDX6 (Figure 6H), which forms complexes with many PB proteins (Ayache et al., 2015; Brandmann et al., 2018; Kamenska et al., 2016; Ohn et al., 2008; Ozgur et al., 2015; Youn et al., 2018). Intriguingly, DDX6 is weakly recruited to SGs in WT cells, whereas other PBs (EDC3 and DCP1A) are repelled (Figure 6I). Remarkably, relative network distance between upregulated nodes correlates with resulting condensate miscibility (Figure 6J): in contrast to neighboring nodes that favor a single miscible phase (e.g., G3BP/UBAP2L, EDC3/DCP1A), simultaneous

Figure 4. High-Valence G3BP RBD Complexes Are Sufficient for Stress Granule Formation with Attached P-Bodies

(A) Corelets allow optogenetic tuning of v_{RBD} (0 to 24) on a 24-subunit Ferritin (Fe) core to mimic endogenous v_{RBD} of G3BP complex. All Corelet experiments (unless noted): v_{RBD} is denoted low (~2-4), medium (~6-8), or high (~18-24); core ~0.25 μM; cells = G3BP KO U2OS.

(B) Reversible G3BP1ΔNTF2 Corelets after 1 h As. Indicated: seconds after oligomerization (+blue light) or monomerization (−blue light), scale bar, 3 μm in all images unless noted.

(C) ΔNTF2 Corelets fuse and relax to a sphere following As, activation (3-min). Scale bar, 2 μm.

(D) FRAP of ΔNTF2 Corelets (+As). Intensity relative to fluorescence before granule bleach. Mean and SEM: n = 8 experiments. Representative images shown, scale bar, 2 μm.

(E) ΔNTF2 Corelet cells (medium *v*) treated with cycloheximide (CH) then As (six 10-min cycles: 5-min activate, 5-min deactivate). Images: after cycle.

(F) Intracellular ΔNTF2 Corelet phase diagrams for drugs that alter available RNA. Each dot = single cell (5-min activation), best-fit phase threshold shown.

(G) Representative images for (F).

(H) Similar to (E) but no CH. Standard deviation of pixel intensity relative to first image shown.

(I) Similar to (F) but for additional As (+/− As; dots shown for +As). Representative images for high *v* cells.

(J) GFP-tagged proteins co-expressed with indicated G3BP Corelets (iLID-Fe lacks GFP tag). Following As and 10-min activation, cells were fixed; arrowheads, PBs attached to SGs. Right: oligo-dT RNA FISH (Corelet, green; polyA+ RNA, magenta).

See also Figure S4.

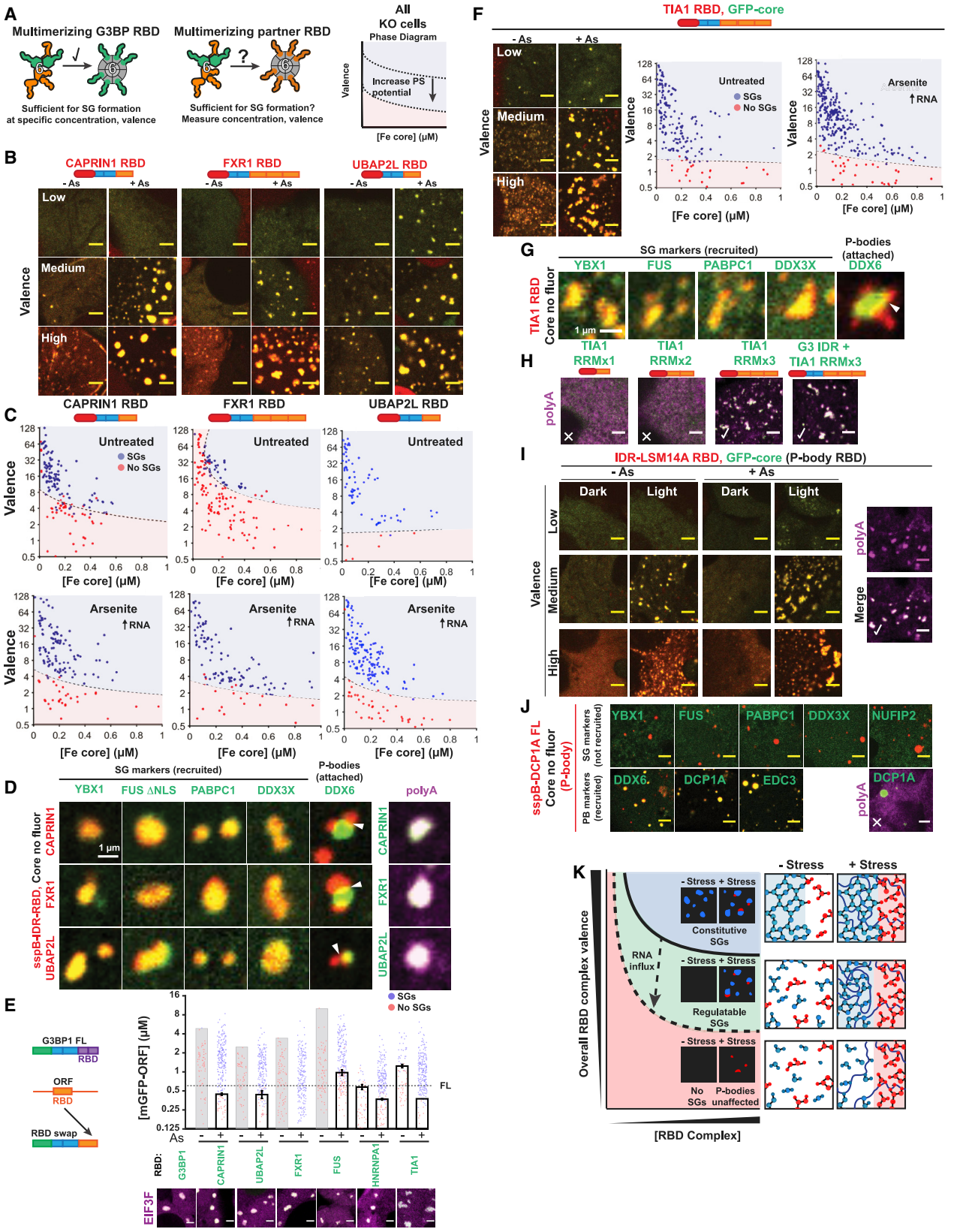

(legend on next page)

overexpression of distant nodes (e.g., G3BP/DCP1A) decouples SGs from PBs (Figures 6K and S7D). This SG/PB dewetting would reflect an increased interfacial tension between the two phases (Feric et al., 2016; Zarzar et al., 2015), which may arise from a decreased relative amount of shared substrate.

Finally, we asked whether competition between nodes with shared preference for the SG RNP network, but unfavorable PPIs, is sufficient for multiphase coexistence. Underscoring the importance of PPIs, co-expression of G3BP NTF2 Corelets (Figure 2B) and NTF2-associated FL SG nodes universally results in a single miscible phase (Figure 6M). In contrast, G3BP RBD (lacking the UBAP2L-binding NTF2 domain) opto-SGs are immiscible with FL UBAP2L granules, forming on their surface and pulling them into close proximity as the multiphase granule grows; upon deactivation, opto-SGs dissolve and attached UBAP2L condensates disperse (Figures 6L). Multiphase coexistence is also observed in a panel of RBD Corelets expressed with their FL node counterparts (Figures 6M and S7E); note in particular how FL UBAP2L forms clear multiphase condensates with all RBD Corelets, likely as a consequence of its additional PPI connectivity to the PB network (Figure 6H). Multiphase coexistence is less apparent for RBD Corelets expressed with FL G3BP, with the exception of CAPRIN1, which results in conspicuous, multiphase SGs (Figure 6M). Since all opto-SGs are compositionally identical in G3BP KO cells (Figures 4 and 5), this result implies that RBD-RNA specificity plays a modulatory role in encoding multiphase coexistence, perhaps by clustering specific RNA sequences with different preferred interactions (Boeynaems et al., 2019; Courel et al., 2019; Fei et al., 2017; Feric et al., 2016; Hubstenberger et al., 2017; Langdon et al., 2018; Moon et al., 2019).

A Minimal Model of PPI Network Phase Behavior Demonstrates Tunable Multiphase Coexistence

Given that many of our experimental findings can be interpreted using valence concepts from the study of patchy colloids, we sought to develop a formal theoretical framework to demonstrate the thermodynamic consistency of our interpretation of the data (Figure 7). Building on prior studies of patchy colloids (Bianchi et al., 2006; Jacobs et al., 2014) and inspired by the endogenous network depicted in Figure 6J, we specified a reduced set of protein complexes with monovalent binding sites, which are allowed to interact according to a prescribed PPI network. We then calculated the conditions for phase coexistence assuming that all interactions have equal affinities (see Quantification and Statistical Analysis). Despite the simplicity of this approach, our minimal model reproduces the key features of tunable multiphase behavior observed in our experiments, including coexisting substrate-dependent and -independent phases (Figure 7A). Eliminating the interactions between two halves of the network by introducing a saturating cap protein (Figure 7B) alters the compositions of the phases and increases the interfacial free-energy barrier between the condensed phases, which tends to suppress wetting (Feric et al., 2016; Zarzar et al., 2015). Reducing the valence of the substrate-binding node by capping the self-interaction sites (Figure 7C) destabilizes the substrate-containing phase. Similarly, removing the substrate inhibits phase separation of the substrate-binding node (Figure 7D). Thus, a minimal patchy-colloids framework is sufficient to describe how tuning the interactions of shared components can contribute to coexisting or disconnected networks in a multiphase system.

DISCUSSION

Cells feature a rich diversity of membraneless condensates, each of which embodies numerous components and coexists with distinct liquid-like compartments (“multiphases”) (Banani et al., 2017; Mao et al., 2011; Nizami et al., 2010; Shin and Brangwynne, 2017). This spatiotemporally dynamic intracellular emulsion reflects the self-assembly output from complex networks of biomolecular interactions. What mechanism might account for multiphase patterning and how is molecular specificity of each condensate encoded? In this work, we have combined biochemical and quantitative intracellular reconstitution approaches with concepts from patchy colloids to introduce a biophysical framework whereby competing RNA-protein networks control multiphase condensation (Figure 7).

In the examined prototype in which cytoplasmic stress granules (SGs) feature attached P-bodies (PBs), G3BP is of critical importance (Bley et al., 2015; Kedersha et al., 2016; Matsuki et al., 2013). Similar to many proteins essential to forming intracellular condensates (e.g., NPM1, nucleolus) (Mitrea and Kriwacki, 2016), G3BP features a modular architecture with a

Figure 5. Stress Granules with Attached P-Bodies Are the Default Multiphase Condensate Encoded by High-Valence RBD Nodes

(A) Corelet assay to test whether NTF2 partners contribute v_{RBD} to G3BP complex.

(B) Valence-dependent condensation (+/−As) examined for indicated RBDs fused to G3BP IDR in Corelet system (images correspond to C). All Corelet experiment images (unless noted): v_{RBD} is noted low (~2–4), medium (~6–8), or high (~18–24); core ~0.25 μM; cells = G3BP KO U2OS; scale bar, 3 μm.

(C) Intracellular phase diagrams for RBDs in (B) +/− As. Each dot = single cell (5-min activation), best-fit phase threshold shown.

(D) GFP-tagged proteins expressed with indicated RBD Corelets (iLID-Fe lacks GFP tag). Following As and 10-min activation, cells were fixed; arrowheads, PBs attached to SGs. Right: oligo-dT RNA FISH.

(E) SG rescue threshold for GFP-tagged chimeric G3BP1 with swapped RBDs (G3BP KO cells with EIF3F-mCh, representative images below). Mean and SEM: n = 4 experiments (>4 images per).

(F) Similar to (B) and (C) but with TIA1 RBD Corelets.

(G) Similar to (D) but with TIA1 RBD Corelets.

(H) Similar to (D) but with TIA1 RBD (number of RRMs altered; +/− G3BP1 IDR).

(I) Similar to (B) and (D) but with RBD from LSM14A (essential PB protein).

(J) Similar to (D) but with DCP1A (PB protein that lacks RBD).

(K) Phase diagram cartoon depicting SG formation as function of nucleating complex concentration and its v_{RBD}. WT cells would exist in green region; G3BP KO/capped, red.

See also Figure S5.

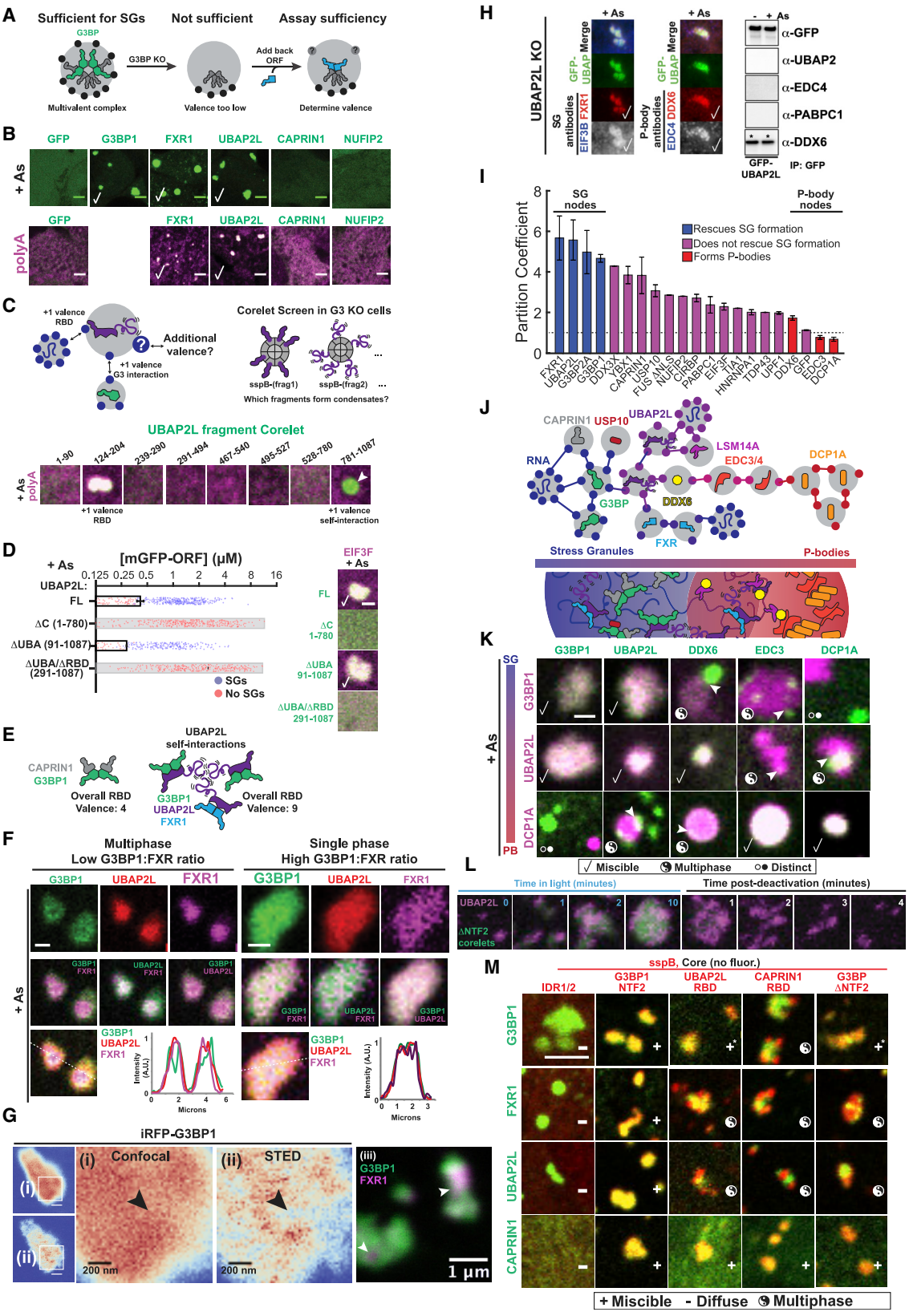

(legend on next page)

dimeric oligomerization domain (OD) and RNA-binding domain (RBD), connected by intrinsically disordered regions (IDRs) (Tourrière et al., 2003; Figures 1A and 1B). Notwithstanding tremendous attention focused on self-associating IDRs in LLPS (Elbaum-Garfinkle et al., 2015; Kato et al., 2012; Lin et al., 2015; Molliex et al., 2015; Nott et al., 2015; Patel et al., 2015; Wang et al., 2018), studies have shown that both ODs and RBDs have essential roles in condensate formation (Feric et al., 2016; Mitrea et al., 2016), including in the case of G3BP-dependent SGs (Bley et al., 2015; Kedersha et al., 2016; Matsuki et al., 2013). Nevertheless, a mechanistic understanding of the contributions of oligomerization, disorder, and RNA binding to multiphase condensation has remained elusive.

Our findings reveal that despite the common assertion that weakly self-associating IDRs are critically important for LLPS, G3BP's IDRs are dispensable for its role in SG assembly (Figure 1), and one should be wary of equating their mere presence with physiological condensation (Riback et al., 2017). Instead, along with two accompanying papers from the Alberti and Taylor labs (Guillén-Boixet et al., 2020; Yang et al., 2020), we uncover a modulatory role for IDRs in tuning the RNA-binding capacity of the associated protein complex and its ability to induce RNP condensation. In the case of G3BP, juxtaposition of its RBD and acidic region (IDR1) prevents RNA engagement and SG assembly. Since similar acidic tracts are found in many SG (e.g., CAPRIN1, FMR1) and nucleolar (e.g., UBTF, NPM1) proteins, such electrostatic-based tuning of RNA-binding affinity may be broadly utilized, and phosphorylation/dephosphorylation of residues near RBDs might toggle RNA-protein interactions (Kim et al., 2019). More in line with recent work (Ruff et al., 2019), we identify a self-associating IDR in UBAP2L that is critical for SG formation. By conferring the ability to weakly interconnect multiple UBAP2L/G3BP and FXR1/UBAP2L complexes, this tyrosine-rich region likely acts as an essential RBD valence multiplier (Figures 6C–6E).

Several studies suggest that dimerization of substrate-binding domains might be sufficient for assembly of certain condensates (Larson et al., 2017; Strom et al., 2017). However, our work highlights the contribution of higher degrees of substrate-binding valence, *v*, and illustrates the importance of careful consideration of ectopic protein expression levels relative to endogenous values in intracellular studies of condensate assembly. Although our experiments are consistent with the assertion that G3BP primarily exists in stress-independent homodimers (Guillén-Boixet et al., 2020; Panas et al., 2015; Schulte et al., 2016; Yang et al., 2020), synthetic RNA-binding dimers are unable to compensate for FL G3BP at physiological concentrations (Figure 1L). Rather, G3BP's dimerization domain (NTF2) must serve as a valence-amplifying interaction platform, recruiting RBD-containing bridges (e.g., CAPRIN1) and secondary nodes (e.g., UBAP2L), the latter of which is also critical for SG assembly (Figure 2). We confirmed the essentiality of such interconnected RBD complexes using an engineered system (Corelets) (Bracha et al., 2018), showing that high-valence G3BP RBD oligomers (nodes) are dramatically more potent than dimers (bridges) at rescuing SG defects in G3BP knockout cells (Figure 4). Importantly, multivalent RBDs of NTF2-associated RBPs (Figure 5) are similarly competent to form PB-studded SGs, a shared preference for the SG RNP network that allows multicomponent G3BP complexes to induce condensation at physiological protein concentrations (Table S1). Such protein complexes (Figures 2 and 6), organized via weakly connected oligomeric nodes, provide sufficient RNA-binding contacts to rapidly condense RNPs into stress granules following polysome disassembly ("RNA influx").

Similarly built interconnected nodes appear to underlie the formation of diverse condensates (Figure 1A), suggesting that such wiring may confer a common evolutionary advantage. Importantly, G3BP's PPI network is conserved in simple metazoans such as *Drosophila* (Baumgartner et al., 2013). Our data suggest a possible rationale for such node-node connectivity (e.g., G3BP-UBAP2L via NTF2) in affording switch-like control of LLPS by ligands (Choi et al., 2019), a mechanism we refer to as "valence capping." NTF2-binding partners (e.g., USP10) that lack RBDs effectively turn G3BP complexes from $v \geq 3$ nodes into $v=2$ bridges, thereby lacking the requisite RNA-binding contacts to condense the SG network (Figure 3). This physical

Figure 6. Competition between Protein-Protein Interaction Nodes Encodes Multiphase Condensation

(A) SG proteins compensate for G3BP if acting as $v>2$ nodes.

(B) Expression (~0.4 μM) of GFP-tagged proteins in G3BP KO cells (+As, oligo-dT RNA FISH). Checks = polyA+ SGs. Scale bar, 3 μm, unless noted.

(C) Corelet screen in G3BP KO cells (+As) to uncover additional valence. Oligo-dT RNA FISH, 10-min activation, fixed. Arrowhead: condensates lack polyA+ mRNA.

(D) G3BP KO cells (+As) expressing GFP-UBAP2LΔs and EIF3F-mCh scored for SGs. Mean and SEM: n = 4 experiments (>4 images per). Images: check = SGs, scale bar, 1 μm.

(E) SG formation requires sufficiently high v_{RBD} complexes, which can be achieved partly via self-associating UBAP2L IDRs (purple tails) in different complexes.

(F) Triple co-expression (GFP-G3BP1, mCh-UBAP2L, iRFP-FXR1) in G3BP KO cells (+As). Line traces for single granules shown. Scale bar, 1 μm.

(G) Super-resolution STED of live G3BP KO cells (+As) with <2 μM of either iRFP-G3BP (left) or GFP-G3BP1 and iRFP-FXR1 (right). Arrowhead: G3BP-depleted regions in SGs.

(H) Left: Immunofluorescence of UBAP2L KO cells (+As) with GFP-UBAP2L. Check = co-localization. Right: IP of GFP-UBAP2L (G3BP KO cells ± As) to detect high-affinity interactions (*).

(I) SG partition coefficients of GFP-tagged proteins in WT cells (+As) with mCh-CAPRIN1. Mean and SEM: n = 3 experiments (n > 4 images per).

(J) Schematic of how protein interaction network may inform molecular mechanism of multi-phase SGs/PBs.

(K) G3BP KO cells (+As) expressing mCh- and GFP-tagged proteins (left to right by network distance from G3BP) pairwise (<2 μM). Legend below. Scale bar, 1 μm.

(L) G3BP KO cells with G3BPΔNTF2 Corelets (green) and UBAP2L-iRFP (<1 μM) were As-treated (1 h) then activated and deactivated.

(M) G3BP KO cells (+As) expressing panel of Corelets (red; untagged core) and GFP-tagged proteins (green, ~2–3 μM); fixed post-activation (10-min). Scale bar, 3 μm.

See also Figures S6 and S7.

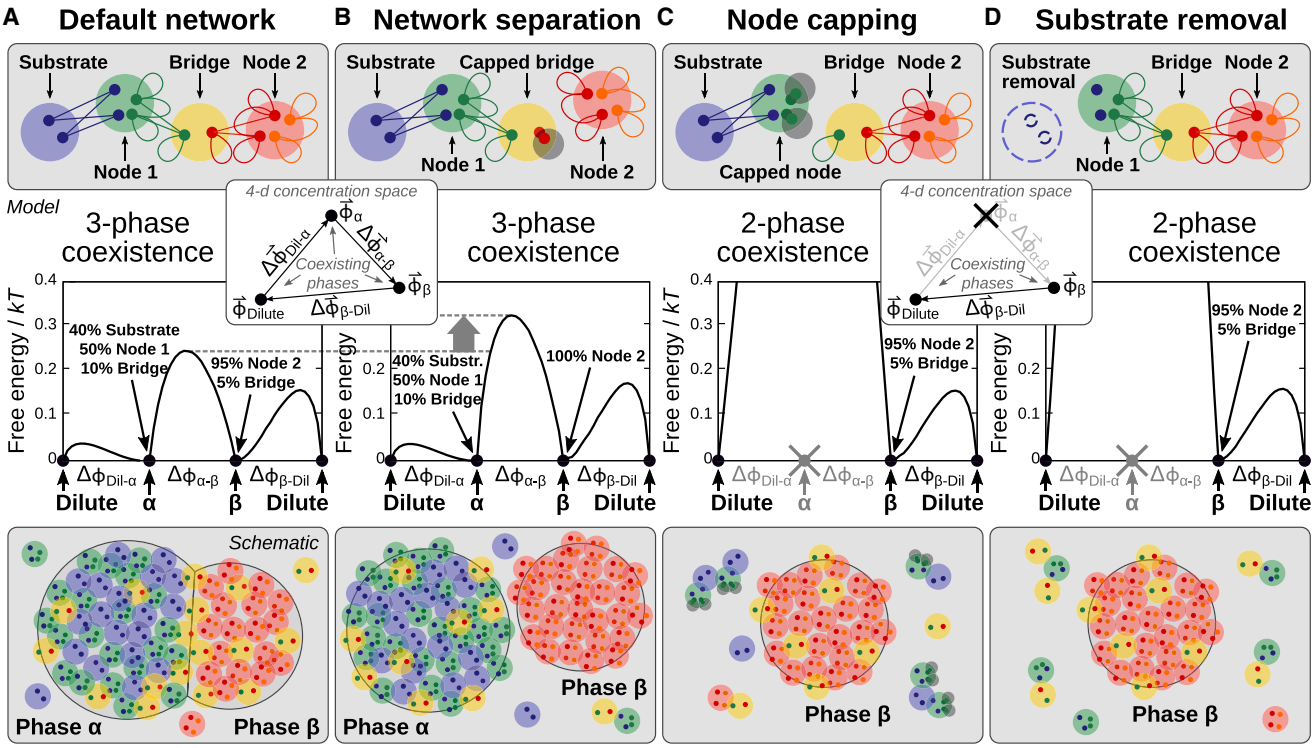

Figure 7. A Minimal Model of PPI Network Phase Behavior Demonstrates Tunable Multiphase Coexistence

(A) A minimal network model consisting of a substrate-binding complex, a bridge complex, and a high-valence self-interacting complex. Top: Large circles represent a single protein, protein complex, or substrate unit; small circles indicate monovalent interaction sites; and lines indicate equal-affinity protein-protein or protein-substrate interactions. Middle: Free-energy landscape calculated at phase coexistence. The coordinate $\Delta\phi$ indicates the distance between a pair of phases, whose compositions are identified above, along a linear path $\Delta\vec{\phi}$. The vertical axis reports the free-energy density in thermal units. Inset: Depiction of the three coexisting phases with concentration vectors $\vec{\phi}$ in a four-dimensional concentration space. Bottom: A cartoon of wetted droplets with a shared component.

(B) Disruption of the Bridge-Node 2 interactions, e.g., via saturation with "cap" proteins, separates the network. The compositions of the α and β phases shift and the α-β interfacial free-energy barrier height increases, which tends to disfavor wetting of the two phases.

(C) Inhibition of the Node 1 self-interactions, e.g., via capping, destabilizes the α phase.

(D) Removal of the substrate also destabilizes the α phase.

model likely represents a broadly applicable framework for understanding how organisms exert spatiotemporal control over phase separation, for example during tissue patterning (Brangwynne et al., 2009; Gammons and Bienz, 2018; Saha et al., 2016; Wu and Fuxreiter, 2016) and condensate spacing (Spencer et al., 2017; Zhang et al., 2018). We speculate that concentrations and composite interaction strengths of interconnected caps, bridges, and nodes have been finely tuned to allow context-dependent "phase switches." In the case of SGs, such a switch is hijacked by diverse viruses to ensure their survival (Panas et al., 2014, 2015; Schulte et al., 2016), which likely reflects a physiological utility (e.g., USP10) (Kedersha et al., 2016; Panas et al., 2015).

Considering the overlap between PB and SG PPI networks (Figure 6J; Youn et al., 2018), another possible evolutionary basis for interconnected nodes is that valence-capping—or ligand-based competition for a node's PPI interfaces more generally—provides a facile way to control directional substrate (e.g., RNA) processing (Kim et al., 2019; Riback et al., 2019). Indeed, we show that subtle manipulation of node stoichiometry causes restructuring of multiphase organization (Figure 6), supporting a biophysical framework in which the relative overlap between networks of interactions (protein-protein, protein-RNA) defines phase immiscibility (or coexistence) and relative RNP partitioning (Figure 7). *De novo* multiphase SGs can result from competition for substrate between a synthetic RBD node and its FL counterpart in an endogenous complex (Figures 6L and 6M). Further, shifting the stoichiometry of highly interconnected nodes is sufficient to encode compositionally distinct hybrid condensates (Figures 6H and 6K), hypertrophied examples of endogenous multiphase SGs (Figures 6F and 6G), or even decoupled SG/PBs (Figure 6K). Thus, competing nodes appear to promote a composition-dependent "tug-of-war" between PPIs and protein-RNA interactions, the outcome of which determines condensate specificity and association (Figure 7). The possibility for even relatively non-overlapping networks to become miscible by shifting the stoichiometric balance highlights the richness of the high-dimensional phase diagrams underlying multiphase condensation (Jacobs and Frenkel, 2017; Mao et al., 2019).

Our results illustrate that, rather than a binary classification scheme for a given multiphase (e.g., SG versus PB), a spectrum

of condensates, each with their own biomolecular composition, is the inevitable consequence of distinct cellular states. Future studies will integrate new experimental findings regarding the caps, nodes, and bridges that define the network connectivity within a given set of condensates, together with theoretical approaches that consider more complex networks of particle-based interactions. In addition to having major implications for substrate processing and organismal development, these efforts will be important for understanding how condensates are manipulated by pathogens to ensure their survival (McInerney, 2015) or pathologies to drive cell death (Freibaum and Taylor, 2017). We envision that such network-based approaches based on soft matter physics will inform the identification of nodes most amenable to therapeutic targeting, and thus inspire new treatment strategies for devastating human diseases.

STAR★METHODS

Detailed methods are provided in the online version of this paper and include the following:

- KEY RESOURCES TABLE
- LEAD CONTACT AND MATERIALS AVAILABILITY
- EXPERIMENTAL MODEL AND SUBJECT DETAILS
- METHOD DETAILS
  - Plasmid construction
  - Generation of lentivirus and lentiviral transduction
  - Transient transfection
  - Microinjections into live U2OS cells
  - Live cell confocal microscopy
  - Stimulated emission depletion (STED) super-resolution microscopy
  - Widefield microscopy
  - Corelet activation
  - Fluorescence recovery after photobleaching (FRAP)
  - Cell treatment with arsenite to dissociate polysomes
  - Inhibition of polysome disassembly by pre-treatment with cycloheximide
  - Cell treatment with Actinomycin D to inhibit transcription
  - Phase diagram data collection
  - Cycling experiments following drug treatments
  - G3BP rescue competition assay and stress granule inhibition experiments
  - Stress granule partitioning
  - Co-Localization Corelet studies
  - RNA fluorescence *in situ* histochemistry (RNA-FISH)
  - Western blot to assess G3BP1/2 levels and knockout
  - Immunoprecipitation of high-affinity protein complexes from U2OS Cells
  - CRISPR-Cas9 generation of KO cell lines and validation
  - Genotyping of Cas9 mutant cell lines
  - Double-positive U2OS stable cell lines
- QUANTIFICATION AND STATISTICAL ANALYSIS
  - Fluorescence correlation spectroscopy
  - Image analysis
  - Manual image segmentation
  - Light-dark cycling experiments
  - G3BP rescue competition data analysis in G3BP KO U2OS cells
  - Phase diagrams and calculation of threshold valence
  - Quantification of threshold concentration for inhibition of stress granule assembly (WT cells) or rescue (G3BP KO cells)
  - Partitioning coefficient image analysis
  - Model of PPI network phase separation
  - Phase coexistence and free-energy landscape calculations
- DATA AND CODE AVAILABILITY

SUPPLEMENTAL INFORMATION

Supplemental Information can be found online at https://doi.org/10.1016/j.cell.2020.03.050.

ACKNOWLEDGMENTS

We thank Rivkah Brown, Chang-Hyun Choi, Evangelos Gatzogiannis, Brittany Grego, Anastasia Repouliou, and Claire Riggs for assistance with experiments, and all Brangwynne Lab members for helpful critiques. We thank J. Paul Taylor (St. Jude Children's Hospital) and Simon Alberti (CMCB/BIOTEC) for discussing independently collected, corroborating data. This work was supported by the Howard Hughes Medical Institute, the St. Jude Research Collaborative on Membrane-less Organelles, the NIH (U01 DA040601), and an NSF CAREER award (125035) (C.P.B.). D.W.S. acknowledges support through the NIH (F32 GM130072); D.S.W.L., NSF Graduate Research Fellowship Program (DCE-1656466); A.R.S., LSRF Fellowship from Mark Foundation For Cancer Research; D.B., Cross-Disciplinary Postdoctoral Fellowship from Human Frontiers Science Program; J.M.E., NWO Rubicon Fellowship; N.K., S.M.L., and P.A., NIH (R35 GM126901); S.M.L., NIH (K99 GM124458); and P.I., NIH (R01 GM126150).

AUTHOR CONTRIBUTIONS

Conceptualization: D.W.S. and C.P.B.; Methodology: D.W.S., N.K., D.S.W.L., V.D., D.B., J.A.R., A.I., M.-T.W., and W.M.J.; Software: D.S.W.L. and W.M.J.; Formal Analysis, D.W.S., N.K., D.S.W.L., J.A.R., D.B., A.W., and W.M.J.; Investigation: D.W.S., N.K., A.R.S., V.D., J.A.R., A.I., A.W., M.-T.W., G.W., and S.M.L.; Resources: D.W.S., N.K., D.S.W.L., A.R.S., V.D., D.B., J.M.E., A.W., and S.M.L.; Writing – Original Draft: D.W.S. and C.P.B.; Writing – Review & Editing: D.W.S., N.K., A.R.S., W.M.J., and C.P.B.; Visualization: D.W.S., A.R.S., and W.M.J.; Supervision and Funding Acquisition, P.A., P.I., and C.P.B.

DECLARATION OF INTERESTS

Patent applications have been filed based on this work.

Received: February 6, 2019
Revised: October 24, 2019
Accepted: March 20, 2020
Published: April 16, 2020

REFERENCES

Adinolfi, S., Ramos, A., Martin, S.R., Dal Piaz, F., Pucci, P., Bardoni, B., Mandel, J.L., and Pastore, A. (2003). The N-terminus of the fragile X mental retardation protein contains a novel domain involved in dimerization and RNA binding. Biochemistry *42*, 10437–10444.

Ayache, J., Bénard, M., Ernoult-Lange, M., Minshall, N., Standart, N., Kress, M., and Weil, D. (2015). P-body assembly requires DDX6 repression

complexes rather than decay or Ataxin2/2L complexes. Mol. Biol. Cell *26*, 2579–2595.

Banani, S.F., Lee, H.O., Hyman, A.A., and Rosen, M.K. (2017). Biomolecular condensates: organizers of cellular biochemistry. Nat. Rev. Mol. Cell Biol. *18*, 285–298.

Baumgartner, R., Stocker, H., and Hafen, E. (2013). The RNA-binding proteins FMR1, rasputin and caprin act together with the UBA protein lingerer to restrict tissue growth in Drosophila melanogaster. PLoS Genet. *9*, e1003598.

Bianchi, E., Blaak, R., and Likos, C.N. (2011). Patchy colloids: state of the art and perspectives. Phys. Chem. Chem. Phys. *13*, 6397–6410.

Bianchi, E., Largo, J., Tartaglia, P., Zaccarelli, E., and Sciortino, F. (2006). Phase diagram of patchy colloids: towards empty liquids. Phys. Rev. Lett. *97*, 168301.

Bley, N., Lederer, M., Pfalz, B., Reinke, C., Fuchs, T., Glaß, M., Möller, B., and Hüttelmaier, S. (2015). Stress granules are dispensable for mRNA stabilization during cellular stress. Nucleic Acids Res. *43*, e26.

Boeynaems, S., Alberti, S., Fawzi, N.L., Mittag, T., Polymenidou, M., Rousseau, F., Schymkowitz, J., Shorter, J., Wolozin, B., Van Den Bosch, L., et al. (2018). Protein Phase Separation: A New Phase in Cell Biology. Trends Cell Biol. *28*, 420–435.

Boeynaems, S., Bogaert, E., Kovacs, D., Konijnenberg, A., Timmerman, E., Volkov, A., Guharoy, M., De Decker, M., Jaspers, T., Ryan, V.H., et al. (2017). Phase Separation of C9orf72 Dipeptide Repeats Perturbs Stress Granule Dynamics. Mol. Cell *65*, 1044–1055.e5.

Boeynaems, S., Holehouse, A.S., Weinhardt, V., Kovacs, D., Van Lindt, J., Larabell, C., Van Den Bosch, L., Das, R., Tompa, P.S., Pappu, R.V., and Gitler, A.D. (2019). Spontaneous driving forces give rise to protein-RNA condensates with coexisting phases and complex material properties. Proc. Natl. Acad. Sci. USA *116*, 7889–7898.

Bounedjah, O., Desforges, B., Wu, T.-D., Pioche-Durieu, C., Marco, S., Hamon, L., Curmi, P.A., Guerquin-Kern, J.-L., Piétrement, O., and Pastré, D. (2014). Free mRNA in excess upon polysome dissociation is a scaffold for protein multimerization to form stress granules. Nucleic Acids Res. *42*, 8678–8691.

Bracha, D., Walls, M.T., Wei, M.-T., Zhu, L., Kurian, M., Avalos, J.L., Toettcher, J.E., and Brangwynne, C.P. (2018). Mapping Local and Global Liquid Phase Behavior in Living Cells Using Photo-Oligomerizable Seeds. Cell *175*, 1467–1480.e13.

Brandmann, T., Fakim, H., Padamsi, Z., Youn, J.-Y., Gingras, A.-C., Fabian, M.R., and Jinek, M. (2018). Molecular architecture of LSM14 interactions involved in the assembly of mRNA silencing complexes. EMBO J. *37*, 9358.

Brangwynne, C.P., Eckmann, C.R., Courson, D.S., Rybarska, A., Hoege, C., Gharakhani, J., Jülicher, F., and Hyman, A.A. (2009). Germline P granules are liquid droplets that localize by controlled dissolution/condensation. Science *324*, 1729–1732.

Brangwynne, C.P., Tompa, P., and Pappu, R.V. (2015). Polymer physics of intracellular phase transitions. Nat. Phys. *11*, 899–904.

Cahn, J.W., and Hilliard, J.E. (1958). Free Energy of a Nonuniform System 0.1. Interfacial Free Energy. J. Chem. Phys. *28*, 258–267.

Chapman, W.G., Gubbins, K.E., Jackson, G., and Radosz, M. (1989). Saft: Equation-of-State Solution Model for Associating Fluids. Fluid Phase Equilib. *52*, 31–38.

Choi, J.-M., Dar, F., and Pappu, R.V. (2019). LASSI: A lattice model for simulating phase transitions of multivalent proteins. PLoS Comput. Biol. *15*, e1007028.

Chong, P.A., Vernon, R.M., and Forman-Kay, J.D. (2018). RGG/RG Motif Regions in RNA Binding and Phase Separation. J. Mol. Biol. *430*, 4650–4665. https://doi.org/10.1016/j.jmb.2018.06.014.

Cirillo, L., Cieren, A., Barbieri, S., Khong, A., Schwager, F., Parker, R., and Gotta, M. (2020). UBAP2L Forms Distinct Cores that Act in Nucleating Stress Granules Upstream of G3BP1. Curr. Biol. *30*, 698–707.e6.

Courel, M., Clément, Y., Bossevain, C., Foretek, D., Vidal Cruchez, O., Yi, Z., Bénard, M., Benassy, M.-N., Kress, M., Vindry, C., et al. (2019). GC content shapes mRNA storage and decay in human cells. eLife *8*, 2579.

de Gennes, P.-G. (2004). Capillarity and wetting phenomena: drops, bubbles, pearls, waves (New York: Springer).

Dolzhanskaya, N., Merz, G., Aletta, J.M., and Denman, R.B. (2006). Methylation regulates the intracellular protein-protein and protein-RNA interactions of FMRP. J. Cell Sci. *119*, 1933–1946.

Elbaum-Garfinkle, S., Kim, Y., Szczepaniak, K., Chen, C.C.-H., Eckmann, C.R., Myong, S., and Brangwynne, C.P. (2015). The disordered P granule protein LAF-1 drives phase separation into droplets with tunable viscosity and dynamics. Proc. Natl. Acad. Sci. USA *112*, 7189–7194.

Eystathioy, T., Chan, E.K.L., Tenenbaum, S.A., Keene, J.D., Griffith, K., and Fritzler, M.J. (2002). A phosphorylated cytoplasmic autoantigen, GW182, associates with a unique population of human mRNAs within novel cytoplasmic speckles. Mol. Biol. Cell *13*, 1338–1351.

Eystathioy, T., Jakymiw, A., Chan, E.K.L., Séraphin, B., Cougot, N., and Fritzler, M.J. (2003). The GW182 protein colocalizes with mRNA degradation associated proteins hDcp1 and hLSm4 in cytoplasmic GW bodies. RNA *9*, 1171–1173.

Fang, M.Y., Markmiller, S., Vu, A.Q., Javaherian, A., Dowdle, W.E., Jolivet, P., Bushway, P.J., Castello, N.A., Baral, A., Chan, M.Y., et al. (2019). Small-Molecule Modulation of TDP-43 Recruitment to Stress Granules Prevents Persistent TDP-43 Accumulation in ALS/FTD. Neuron *103*, 802–819.e11.

Fei, J., Jadaliha, M., Harmon, T.S., Li, I.T.S., Hua, B., Hao, Q., Holehouse, A.S., Reyer, M., Sun, Q., Freier, S.M., et al. (2017). Quantitative analysis of multilayer organization of proteins and RNA in nuclear speckles at super resolution. J. Cell Sci. *130*, 4180–4192.

Feric, M., Vaidya, N., Harmon, T.S., Mitrea, D.M., Zhu, L., Richardson, T.M., Kriwacki, R.W., Pappu, R.V., and Brangwynne, C.P. (2016). Coexisting Liquid Phases Underlie Nucleolar Subcompartments. Cell *165*, 1686–1697.

Freibaum, B.D., and Taylor, J.P. (2017). The Role of Dipeptide Repeats in C9ORF72-Related ALS-FTD. Front. Mol. Neurosci. *10*, 35.

Frey, S., Richter, R.P., and Görlich, D. (2006). FG-rich repeats of nuclear pore proteins form a three-dimensional meshwork with hydrogel-like properties. Science *314*, 815–817.

Gammons, M., and Bienz, M. (2018). Multiprotein complexes governing Wnt signal transduction. Curr. Opin. Cell Biol. *51*, 42–49.

Guillén-Boixet, J., Kopach, A., Holehouse, A.S., Wittmann, S., Jahnel, M., Schlüßler, R., Kim, K., Trussina, I.R.E.A., Wang, J., Mateju, D., et al. (2020). RNA-induced conformational switching and clustering of G3BP drive stress granule assembly by condensation. Cell *181*, 346–361.

Guntas, G., Hallett, R.A., Zimmerman, S.P., Williams, T., Yumerefendi, H., Bear, J.E., and Kuhlman, B. (2015). Engineering an improved light-induced dimer (iLID) for controlling the localization and activity of signaling proteins. Proc. Natl. Acad. Sci. USA *112*, 112–117.

Guo, X., Wang, H., Li, Y., Leng, X., Huang, W., Ma, Y., Xu, T., and Qi, X. (2019). Transfection reagent Lipofectamine triggers type I interferon signaling activation in macrophages. Immunol. Cell Biol. *97*, 92–96.

Hagen, L., Sharma, A., Aas, P.A., and Slupphaug, G. (2015). Off-target responses in the HeLa proteome subsequent to transient plasmid-mediated transfection. Biochim. Biophys. Acta *1854*, 84–90.

Hein, M.Y., Hubner, N.C., Poser, I., Cox, J., Nagaraj, N., Toyoda, Y., Gak, I.A., Weisswange, I., Mansfeld, J., Buchholz, F., et al. (2015). A human interactome in three quantitative dimensions organized by stoichiometries and abundances. Cell *163*, 712–723.

Huang, C., Chen, Y., Dai, H., Zhang, H., Xie, M., Zhang, H., Chen, F., Kang, X., Bai, X., and Chen, Z. (2020). UBAP2L arginine methylation by PRMT1 modulates stress granule assembly. Cell Death Differ. *27*, 227–241.

Hubstenberger, A., Courel, M., Bénard, M., Souquere, S., Ernoult-Lange, M., Chouaib, R., Yi, Z., Morlot, J.-B., Munier, A., Fradet, M., et al. (2017). P-Body Purification Reveals the Condensation of Repressed mRNA Regulons. Mol. Cell *68*, 144–157.e5.

Ivanov, P., Kedersha, N., and Anderson, P. (2019). Stress Granules and Processing Bodies in Translational Control. Cold Spring Harb. Perspect. Biol *11*. https://doi.org/10.1101/cshperspect.a032813.

Jacobs, W.M., and Frenkel, D. (2017). Phase Transitions in Biological Systems with Many Components. Biophys. J. *112*, 683–691.

Jacobs, W.M., Oxtoby, D.W., and Frenkel, D. (2014). Phase separation in solutions with specific and nonspecific interactions. J. Chem. Phys. *140*, 204109.

Jain, S., Wheeler, J.R., Walters, R.W., Agrawal, A., Barsic, A., and Parker, R. (2016). ATPase-Modulated Stress Granules Contain a Diverse Proteome and Substructure. Cell *164*, 487–498.

Kamenska, A., Simpson, C., Vindry, C., Broomhead, H., Bénard, M., Ernoult-Lange, M., Lee, B.P., Harries, L.W., Weil, D., and Standart, N. (2016). The DDX6-4E-T interaction mediates translational repression and P-body assembly. Nucleic Acids Res. *44*, 6318–6334.

Kato, M., Han, T.W., Xie, S., Shi, K., Du, X., Wu, L.C., Mirzaei, H., Goldsmith, E.J., Longgood, J., Pei, J., et al. (2012). Cell-free formation of RNA granules: low complexity sequence domains form dynamic fibers within hydrogels. Cell *149*, 753–767.

Kedersha, N., Chen, S., Gilks, N., Li, W., Miller, I.J., Stahl, J., and Anderson, P. (2002). Evidence that ternary complex (eIF2-GTP-tRNA(i)(Met))-deficient preinitiation complexes are core constituents of mammalian stress granules. Mol. Biol. Cell *13*, 195–210.

Kedersha, N.L., Gupta, M., Li, W., Miller, I., and Anderson, P. (1999). RNA-binding proteins TIA-1 and TIAR link the phosphorylation of eIF-2 alpha to the assembly of mammalian stress granules. J. Cell Biol. *147*, 1431–1442.

Kedersha, N., Panas, M.D., Achorn, C.A., Lyons, S., Tisdale, S., Hickman, T., Thomas, M., Lieberman, J., McInerney, G.M., Ivanov, P., and Anderson, P. (2016). G3BP-Caprin1-USP10 complexes mediate stress granule condensation and associate with 40S subunits. J. Cell Biol. *212*, 845–860.

Kedersha, N., Stoecklin, G., Ayodele, M., Yacono, P., Lykke-Andersen, J., Fritzler, M.J., Scheuner, D., Kaufman, R.J., Golan, D.E., and Anderson, P. (2005). Stress granules and processing bodies are dynamically linked sites of mRNP remodeling. J. Cell Biol. *169*, 871–884.

Kim, T.H., Tsang, B., Vernon, R.M., Sonenberg, N., Kay, L.E., and Forman-Kay, J.D. (2019). Phospho-dependent phase separation of FMRP and CAPRIN1 recapitulates regulation of translation and deadenylation. Science *365*, 825–829.

Kristensen, O. (2015). Crystal structure of the G3BP2 NTF2-like domain in complex with a canonical FGDF motif peptide. Biochem. Biophys. Res. Commun. *467*, 53–57.

Kroschwald, S., Maharana, S., Mateju, D., Malinovska, L., Nüske, E., Poser, I., Richter, D., and Alberti, S. (2015). Promiscuous interactions and protein disaggregases determine the material state of stress-inducible RNP granules. eLife *4*, e06807.

Langdon, E.M., Qiu, Y., Ghanbari Niaki, A., McLaughlin, G.A., Weidmann, C.A., Gerbich, T.M., Smith, J.A., Crutchley, J.M., Termini, C.M., Weeks, K.M., et al. (2018). mRNA structure determines specificity of a polyQ-driven phase separation. Science *360*, 922–927.

Larson, A.G., Elnatan, D., Keenen, M.M., Trnka, M.J., Johnston, J.B., Burlingame, A.L., Agard, D.A., Redding, S., and Narlikar, G.J. (2017). Liquid droplet formation by HP1α suggests a role for phase separation in heterochromatin. Nature *547*, 236–240.

Li, P., Banjade, S., Cheng, H.-C., Kim, S., Chen, B., Guo, L., Llaguno, M., Hollingsworth, J.V., King, D.S., Banani, S.F., et al. (2012). Phase transitions in the assembly of multivalent signalling proteins. Nature *483*, 336–340.

Lin, Y., Protter, D.S.W., Rosen, M.K., and Parker, R. (2015). Formation and Maturation of Phase-Separated Liquid Droplets by RNA-Binding Proteins. Mol. Cell *60*, 208–219.

Maharana, S., Wang, J., Papadopoulos, D.K., Richter, D., Pozniakovsky, A., Poser, I., Bickle, M., Rizk, S., Guillén-Boixet, J., Franzmann, T.M., et al. (2018). RNA buffers the phase separation behavior of prion-like RNA binding proteins. Science *360*, 918–921.

Mao, S., Kuldinow, D., Haataja, M.P., and Košmrlj, A. (2019). Phase behavior and morphology of multicomponent liquid mixtures. Soft Matter *15*, 1297–1311.

Mao, Y.S., Zhang, B., and Spector, D.L. (2011). Biogenesis and function of nuclear bodies. Trends Genet. *27*, 295–306.

Markmiller, S., Soltanieh, S., Server, K.L., Mak, R., Jin, W., Fang, M.Y., Luo, E.-C., Krach, F., Yang, D., Sen, A., et al. (2018). Context-Dependent and Disease-Specific Diversity in Protein Interactions within Stress Granules. Cell *172*, 590–604.e13.

Matsuki, H., Takahashi, M., Higuchi, M., Makokha, G.N., Oie, M., and Fujii, M. (2013). Both G3BP1 and G3BP2 contribute to stress granule formation. Genes Cells *18*, 135–146.

McInerney, G.M. (2015). FGDF motif regulation of stress granule formation. DNA Cell Biol. *34*, 557–560.

Michelsen, M.L., and Hendriks, E.M. (2001). Physical properties from association models. Fluid Phase Equilib. *180*, 165–174.

Mitrea, D.M., Cika, J.A., Guy, C.S., Ban, D., Banerjee, P.R., Stanley, C.B., Nourse, A., Deniz, A.A., and Kriwacki, R.W. (2016). Nucleophosmin integrates within the nucleolus via multi-modal interactions with proteins displaying R-rich linear motifs and rRNA. eLife *5*, D181.

Mitrea, D.M., and Kriwacki, R.W. (2016). Phase separation in biology; functional organization of a higher order. Cell Commun. Signal. *14*, 1.

Molliex, A., Temirov, J., Lee, J., Coughlin, M., Kanagaraj, A.P., Kim, H.J., Mittag, T., and Taylor, J.P. (2015). Phase separation by low complexity domains promotes stress granule assembly and drives pathological fibrillization. Cell *163*, 123–133.

Moon, S.L., Morisaki, T., Khong, A., Lyon, K., Parker, R., and Stasevich, T.J. (2019). Multicolour single-molecule tracking of mRNA interactions with RNP granules. Nat. Cell Biol. *21*, 162–168.

Niewidok, B., Igaev, M., Pereira da Graca, A., Strassner, A., Lenzen, C., Richter, C.P., Piehler, J., Kurre, R., and Brandt, R. (2018). Single-molecule imaging reveals dynamic biphasic partition of RNA-binding proteins in stress granules. J. Cell Biol. *217*, 1303–1318.

Nizami, Z., Deryusheva, S., and Gall, J.G. (2010). The Cajal body and histone locus body. Cold Spring Harb. Perspect. Biol. *2*, a000653.

Nott, T.J., Petsalaki, E., Farber, P., Jervis, D., Fussner, E., Plochowietz, A., Craggs, T.D., Bazett-Jones, D.P., Pawson, T., Forman-Kay, J.D., and Baldwin, A.J. (2015). Phase transition of a disordered nuage protein generates environmentally responsive membraneless organelles. Mol. Cell *57*, 936–947.

Ohn, T., Kedersha, N., Hickman, T., Tisdale, S., and Anderson, P. (2008). A functional RNAi screen links O-GlcNAc modification of ribosomal proteins to stress granule and processing body assembly. Nat. Cell Biol. *10*, 1224–1231.

Ozgur, S., Basquin, J., Kamenska, A., Filipowicz, W., Standart, N., and Conti, E. (2015). Structure of a Human 4E-T/DDX6/CNOT1 Complex Reveals the Different Interplay of DDX6-Binding Proteins with the CCR4-NOT Complex. Cell Rep. *13*, 703–711.

Panas, M.D., Ahola, T., and McInerney, G.M. (2014). The C-terminal repeat domains of nsP3 from the Old World alphaviruses bind directly to G3BP. J. Virol. *88*, 5888–5893.

Panas, M.D., Kedersha, N., Schulte, T., Branca, R.M., Ivanov, P., and Anderson, P. (2019). Phosphorylation of G3BP1-S149 does not influence stress granule assembly. J. Cell Biol. *218*, 2425–2432.

Panas, M.D., Schulte, T., Thaa, B., Sandalova, T., Kedersha, N., Achour, A., and McInerney, G.M. (2015). Viral and cellular proteins containing FGDF motifs bind G3BP to block stress granule formation. PLoS Pathog. *11*, e1004659.

Patel, A., Lee, H.O., Jawerth, L., Maharana, S., Jahnel, M., Hein, M.Y., Stoynov, S., Mahamid, J., Saha, S., Franzmann, T.M., et al. (2015). A Liquid-to-Solid Phase Transition of the ALS Protein FUS Accelerated by Disease Mutation. Cell *162*, 1066–1077.

Protter, D.S.W., and Parker, R. (2016). Principles and Properties of Stress Granules. Trends Cell Biol. *26*, 668–679.

Riback, J.A., Katanski, C.D., Kear-Scott, J.L., Pilipenko, E.V., Rojek, A.E., Sosnick, T.R., and Drummond, D.A. (2017). Stress-Triggered Phase Separation Is an Adaptive, Evolutionarily Tuned Response. Cell *168*, 1028–1040.e19.

Riback, J.A., Zhu, L., Ferrolino, M.C., Tolbert, M., Mitrea, D.M., Sanders, D.W., Wei, M.-T., Kriwacki, R.W., and Brangwynne, C.P. (2019). Composition dependent phase separation underlies directional flux through the nucleolus. bioRxiv. https://doi.org/10.1101/809210.

Rollins, C.T., Rivera, V.M., Woolfson, D.N., Keenan, T., Hatada, M., Adams, S.E., Andrade, L.J., Yaeger, D., van Schravendijk, M.R., Holt, D.A., et al. (2000). A ligand-reversible dimerization system for controlling protein-protein interactions. Proc. Natl. Acad. Sci. USA *97*, 7096–7101.

Rubinstein, M. (2003). Polymer physics (New York: Oxford University Press).

Ruff, K.M., Pappu, R.V., and Holehouse, A.S. (2019). Conformational preferences and phase behavior of intrinsically disordered low complexity sequences: insights from multiscale simulations. Curr. Opin. Struct. Biol. *56*, 1–10.

Saha, S., Weber, C.A., Nousch, M., Adame-Arana, O., Hoege, C., Hein, M.Y., Osborne-Nishimura, E., Mahamid, J., Jahnel, M., Jawerth, L., et al. (2016). Polar Positioning of Phase-Separated Liquid Compartments in Cells Regulated by an mRNA Competition Mechanism. Cell *166*, 1572–1584.e16.

Sanders, D.W., Kaufman, S.K., DeVos, S.L., Sharma, A.M., Mirbaha, H., Li, A., Barker, S.J., Foley, A.C., Thorpe, J.R., Serpell, L.C., et al. (2014). Distinct tau prion strains propagate in cells and mice and define different tauopathies. Neuron *82*, 1271–1288.

Schaefer, K.N., and Peifer, M. (2019). Wnt/Beta-Catenin Signaling Regulation and a Role for Biomolecular Condensates. Dev. Cell *48*, 429–444.

Schulte, T., Liu, L., Panas, M.D., Thaa, B., Dickson, N., Götte, B., Achour, A., and McInerney, G.M. (2016). Combined structural, biochemical and cellular evidence demonstrates that both FGDF motifs in alphavirus nsP3 are required for efficient replication. Open Biol. *6*, 160078.

Shalem, O., Sanjana, N.E., Hartenian, E., Shi, X., Scott, D.A., Mikkelson, T., Heckl, D., Ebert, B.L., Root, D.E., Doench, J.G., and Zhang, F. (2014). Genome-scale CRISPR-Cas9 knockout screening in human cells. Science *343*, 84–87.

Shin, Y., Berry, J., Pannucci, N., Haataja, M.P., Toettcher, J.E., and Brangwynne, C.P. (2017). Spatiotemporal Control of Intracellular Phase Transitions Using Light-Activated optoDroplets. Cell *168*, 159–171.e14.

Shin, Y., and Brangwynne, C.P. (2017). Liquid phase condensation in cell physiology and disease. Science *357*. https://doi.org/10.1126/science.aaf4382.

Solomon, S., Xu, Y., Wang, B., David, M.D., Schubert, P., Kennedy, D., and Schrader, J.W. (2007). Distinct structural features of caprin-1 mediate its interaction with G3BP-1 and its induction of phosphorylation of eukaryotic translation initiation factor 2alpha, entry to cytoplasmic stress granules, and selective interaction with a subset of mRNAs. Mol. Cell. Biol. *27*, 2324–2342.

Souquere, S., Mollet, S., Kress, M., Dautry, F., Pierron, G., and Weil, D. (2009). Unravelling the ultrastructure of stress granules and associated P-bodies in human cells. J. Cell Sci. *122*, 3619–3626.

Spencer, A.K., Schaumberg, A.J., and Zallen, J.A. (2017). Scaling of cytoskeletal organization with cell size in *Drosophila*. Mol. Biol. Cell *28*, 1519–1529.

Strom, A.R., Emelyanov, A.V., Mir, M., Fyodorov, D.V., Darzacq, X., and Karpen, G.H. (2017). Phase separation drives heterochromatin domain formation. Nature *547*, 241–245.

Tauber, D., Tauber, G., Khong, A., Van Treeck, B., Pelletier, J., and Parker, R. (2020). Modulation of RNA Condensation by the DEAD-Box Protein eIF4A. Cell *180*, 411–426.e16.

Thandapani, P., O'Connor, T.R., Bailey, T.L., and Richard, S. (2013). Defining the RGG/RG motif. Mol. Cell *50*, 613–623.

Tourrière, H., Chebli, K., Zekri, L., Courselaud, B., Blanchard, J.M., Bertrand, E., and Tazi, J. (2003). The RasGAP-associated endoribonuclease G3BP assembles stress granules. J. Cell Biol. *160*, 823–831.

Vognsen, T., Møller, I.R., and Kristensen, O. (2013). Crystal structures of the human G3BP1 NTF2-like domain visualize FxFG Nup repeat specificity. PLoS ONE *8*, e80947.

Wang, J., Choi, J.-M., Holehouse, A.S., Lee, H.O., Zhang, X., Jahnel, M., Maharana, S., Lemaitre, R., Pozniakovsky, A., Drechsel, D., et al. (2018). A Molecular Grammar Governing the Driving Forces for Phase Separation of Prion-like RNA Binding Proteins. Cell *174*, 688–699.e16.

Wheeler, J.R., Matheny, T., Jain, S., Abrisch, R., and Parker, R. (2016). Distinct stages in stress granule assembly and disassembly. eLife *5*, 875.

Wippich, F., Bodenmiller, B., Trajkovska, M.G., Wanka, S., Aebersold, R., and Pelkmans, L. (2013). Dual specificity kinase DYRK3 couples stress granule condensation/dissolution to mTORC1 signaling. Cell *152*, 791–805.

Wolff, J., Marques, C.M., and Thalmann, F. (2011). Thermodynamic approach to phase coexistence in ternary phospholipid-cholesterol mixtures. Phys. Rev. Lett. *106*, 128104.

Wu, H., and Fuxreiter, M. (2016). The Structure and Dynamics of Higher-Order Assemblies: Amyloids, Signalosomes, and Granules. Cell *165*, 1055–1066.

Yang, P., Mathieu, C., Kolaitis, R.M., Zhang, P., Messing, J., Yurtsever, U., Yang, Z., Wu, J., Li, Y., Pan, Q., et al. (2020). G3BP1 is a tunable switch that triggers phase separation to assemble stress granules. Cell *181*, 325–345.

Youn, J.-Y., Dunham, W.H., Hong, S.J., Knight, J.D.R., Bashkurov, M., Chen, G.I., Bagci, H., Rathod, B., MacLeod, G., Eng, S.W.M., et al. (2018). High-Density Proximity Mapping Reveals the Subcellular Organization of mRNA-Associated Granules and Bodies. Mol. Cell *69*, 517–532.e11.

Youn, J.-Y., Dyakov, B.J.A., Zhang, J., Knight, J.D.R., Vernon, R.M., Forman-Kay, J.D., and Gingras, A.-C. (2019). Properties of Stress Granule and P-Body Proteomes. Mol. Cell *76*, 286–294.

Zarzar, L.D., Sresht, V., Sletten, E.M., Kalow, J.A., Blankschtein, D., and Swager, T.M. (2015). Dynamically reconfigurable complex emulsions via tunable interfacial tensions. Nature *518*, 520–524.

Zhang, P., Fan, B., Yang, P., Temirov, J., Messing, J., Kim, H.J., and Taylor, J.P. (2019). Chronic optogenetic induction of stress granules is cytotoxic and reveals the evolution of ALS-FTD pathology. eLife *8*, 651.

Zhang, L., Köhler, S., Rillo-Bohn, R., and Dernburg, A.F. (2018). A compartmentalized signaling network mediates crossover control in meiosis. eLife *7*, 245.

Zhu, L., and Brangwynne, C.P. (2015). Nuclear bodies: the emerging biophysics of nucleoplasmic phases. Curr. Opin. Cell Biol. *34*, 23–30.